

## Dephasing by electron–electron interactions in a ballistic Mach–Zehnder interferometer

**Clemens Neuenhahn and Florian Marquardt**

Department of Physics, Arnold Sommerfeld Center for Theoretical Physics,  
and Center for NanoScience, Ludwig Maximilians Universität München,  
Theresienstrasse 37, 80333 Munich, Germany

E-mail: [clemens.neuenhahn@physik.uni-muenchen.de](mailto:clemens.neuenhahn@physik.uni-muenchen.de)

*New Journal of Physics* **10** (2008) 115018 (32pp)

Received 18 June 2008

Published 20 November 2008

Online at <http://www.njp.org/>

doi:10.1088/1367-2630/10/11/115018

**Abstract.** We consider a ballistic Mach–Zehnder interferometer for electrons propagating chirally in one dimension (such as in an integer quantum Hall effect edge channel). In such a system, dephasing occurs when the finite range of the interaction potential is taken into account. Using the tools of bosonization, we discuss the decay of coherence as a function of propagation distance and energy. We supplement the exact solution by a semiclassical approach that is physically transparent and is exact at high energies. In particular, we study in more detail the recently predicted universal power-law decay of the coherence at high energies, where the exponent does not depend on the interaction strength. In addition, we compare against Keldysh perturbation theory, which works well for small interaction strength at short propagation distances.

**Contents**

<b>1. Introduction</b>	<b>2</b>
<b>2. The electronic Mach–Zehnder interferometer</b>	<b>5</b>
2.1. Current . . . . .	5
2.2. Evaluation of the current . . . . .	7
2.3. Visibility . . . . .	9
<b>3. Solution by bosonization</b>	<b>9</b>
3.1. Hamiltonian and formal solution . . . . .	9
3.2. GF from bosonization . . . . .	11
3.3. Discussion: GF in space and time . . . . .	12
3.4. GF versus position and energy . . . . .	13
3.5. Large coupling constants . . . . .	14
<b>4. Semiclassical model of dephasing</b>	<b>15</b>
4.1. Semiclassical approach to the GF . . . . .	16
4.2. Universal dephasing for high-energy electrons . . . . .	20
<b>5. Keldysh perturbation theory</b>	<b>23</b>
5.1. General remarks . . . . .	23
5.2. Evaluation of the diagrams . . . . .	24
5.3. Summary of the Keldysh perturbation theory . . . . .	27
<b>6. Visibility and current</b>	<b>27</b>
<b>7. Conclusions</b>	<b>28</b>
<b>Acknowledgments</b>	<b>28</b>
<b>Appendix A. Semiclassical approach</b>	<b>28</b>
<b>Appendix B. Keldysh perturbation theory: vertex correction</b>	<b>30</b>
<b>References</b>	<b>30</b>

**1. Introduction**

The loss of quantum mechanical phase coherence by a fluctuating environment plays an essential role in many different branches of modern physics [1]. It governs the transition from the quantum to the classical world [2, 3] and occurs as an unavoidable consequence of any measurement process [4]. It introduces the dephasing time as the timescale during which it is possible to observe quantum coherent dynamics in qubits and other quantum objects. Furthermore, the interference contrast in man-made interferometers is determined by decoherence. This includes setups for electrons in semiconductors or metals, for single photons, neutrons, neutral atoms and larger objects. In each of those examples various different sources of fluctuations contribute, e.g. thermal radiation, or the interaction with phonons and other particles.

The paradigmatic setup that is treated in much of the literature on decoherence is the following: a ‘small’ quantum system with few degrees of freedom or even a finite-dimensional Hilbert space (atom, spin, qubit and single particle) interacts with an equilibrium environment that comprises an infinite number of degrees of freedom, i.e. a ‘bath’. In the majority of cases, the model of the environment is restricted even further, to consist of a collection of harmonic

oscillators (e.g. photon or phonon modes). Quantum dissipative systems of that kind already offer a rich phenomenology, including exponential or power-law decay of the coherence in time, as well as dissipative phase transitions at strong coupling [1, 5].

However, there are several situations in which one is forced to go beyond that class of models. We mention three of the most important examples, where the nature of the environment has to be reconsidered. (i) The environment may be driven out of equilibrium (as in the interaction with electrical currents or a photon stream emanating from a laser), which is particularly important for measurement setups. As a consequence, extra fluctuations are introduced and there is no simple relation any more between the dissipative response and the fluctuations. (ii) The environment may be different from a bath of harmonic oscillators, such that the resulting fluctuations are not Gaussian. This comprises examples like spin baths, fluctuators in solids, or potential fluctuations being produced by discrete particles, such as electrons. The peculiar features of non-Gaussian environments may be observed at strong coupling, and they include oscillations of the interference contrast with time [6, 7]. (iii) It may be hard to cleanly separate (conceptually and technically) the environment from the system. This is the case for interacting many-particle systems, where one is interested in the effects on a single particle that is part of the whole, being indistinguishable from the other particles.

In this paper, we will address the third case, which is important in a variety of electronic systems, ranging from dephasing in disordered conductors to electronic interferometers. Here, we will focus on interacting electrons moving inside a ballistic interferometer, although we also would like to mention our recent related work on the importance of Pauli blocking for dephasing in disordered electron systems [8]–[10]. More specifically, we will discuss the loss of coherence in an interacting one-dimensional (1D) chiral fermion system. Besides representing an exactly solvable model system, where one is not restricted to perturbation theory in the interaction, this also has become relevant for experiments recently. In a series of experimental studies [11]–[15], first initiated at the Weizmann institute, an electronic Mach–Zehnder interferometer has been realized, employing edge channels in the integer quantum Hall effect (QHE). The interference contrast as a function of voltage and temperature has been analyzed, and only a fraction of the features have been explained up to now.

On the theoretical side, dephasing in such a setup has been discussed both for dephasing by external fluctuations [6, 13], [16]–[21] (such as phonons, defect fluctuators or Nyquist noise from external gates, or ‘dephasing terminal’ reservoirs), as well as by the intrinsic electron–electron interaction [6], [22]–[27].

Electron–electron interactions in 1D systems are usually described within the Luttinger liquid framework. Dephasing of electrons in Luttinger liquids is interesting as an example of a non-perturbative, strongly correlated model system, and has been studied already in a number of works [28]–[33]. In contrast, the situation for (spinless) chiral interacting fermion systems, such as edge states in the integer QHE, seems to be straightforward. Within the commonly discussed ‘*g*-ology’ framework, one assumes pointlike interactions. In that case, an interacting chiral model is nothing but a Fermi gas with a renormalized velocity. No further interaction effects are present, in particular there is no dephasing. However, for interferometers in nonequilibrium (at finite bias voltage) or at finite temperatures, one may still encounter interesting physics, provided the finite range of the interaction potential is accounted for. This was discussed only recently [25], although there are some nice and thorough earlier studies [34, 35] of the momentum-resolved density of states in such systems.

In the present paper, we build on the recent analysis of Chalker *et al* [25]. These authors modeled the interacting Mach–Zehnder interferometer as consisting of two 1D chiral interacting fermion systems, corresponding to the two channels or arms of the interferometer. The two channels are tunnel-coupled weakly at two locations, representing the quantum point contacts (QPCs) (i.e. the beam splitters) of the experimental setup. By staying within the regime of weak tunnel coupling (low transmission), one is able to express the current in lowest order perturbation theory with regard to the tunneling. The result is a formula for the current (and subsequently, the interference contrast or ‘visibility’) that only involves the Green’s functions (GFs) of the interacting channels in the absence of tunneling. These GFs can be obtained using the tools of bosonization. In order to obtain nontrivial results, it is necessary to go beyond the commonly employed assumption of pointlike interactions. Only when treating the full dependence of the interaction potential on the distance of the electrons, are interaction effects beyond a simple velocity renormalization observed. The main results of their study are that at low voltages and temperatures the interference contrast becomes perfect, while the suppression of contrast at increasing voltages and temperatures depends on the details of the interaction potential.

In our work, we will first review the general expression for the current that consists of two parts, a flux-independent term and the interference contribution that will be suppressed by interaction-induced decoherence (section 2). In contrast to [25], we formulate the answer in terms of the GF in energy-position space. This has the advantage of corresponding directly to the contribution of an electron at energy  $\epsilon$  that travels a distance  $x$  inside one of the arms of the interferometer. Next, we review the model Hamiltonian and the solution by bosonization (section 3). We discuss the general features of the GF  $|G^>(\epsilon, x)|$  that has been obtained by numerical evaluation of the exact bosonization expressions, and study the influence of the coupling constant. At low energies, the decay with propagation distance  $x$  is weak. It becomes faster when the energy rises above the characteristic energy that characterizes the finite range of the interaction. Finally, at large energies, the decay becomes independent of energy.

The latter asymptotic regime is then the subject of a more detailed analysis using a physically transparent semiclassical picture (section 4). This picture of a single electron interacting with the potential fluctuations produced by the other electrons has been exploited by us in a recent short paper [36] to discuss dephasing in an interacting chiral fermion system. It had been introduced earlier to deal with dephasing of ballistically propagating electrons in contact with an arbitrary quantum environment [17, 21], and has also been suggested independently in the context of two interacting Luttinger liquids [30]. Here, we provide more details of the calculation and an extended discussion of the fluctuation spectrum that is seen by the moving electron in its frame of reference. One of the main results is that at high energies there is a ‘universal’ power-law decay  $|G^>(\epsilon, x)| \propto 1/x$  of the electron’s coherence, with an exponent independent of interaction strength. We also analyze the situation at finite temperature, where one has to discuss the transformation of the lab-frame temperature into an effective temperature in the co-moving frame of reference.

Although in principle, for this particular problem, the bosonization solution is fully sufficient, we conclude our analysis with a section on perturbation theory (section 5). This is done in anticipation of going to different setups where an exact solution is no longer possible. Even though we will only discuss the equilibrium GF of the interacting system, we employ the nonequilibrium (Keldysh) diagrammatic technique, to provide for a straightforward extension to situations where this is needed. We calculate the self-energy up to second order in the

interaction. This includes a diagram that describes the decay by emission of a plasmonic excitation, which is however partially cancelled at low energies by an exchange-type diagram. We will show that at short propagation distances and for modest coupling strengths, the Keldysh result provides a good approximation to the exact solution for  $|G^>(\epsilon, x)|$ , even though its structure in  $(\epsilon, k)$ -space is qualitatively different from the bosonization result.

## 2. The electronic Mach–Zehnder interferometer

The electronic Mach–Zehnder interferometer is one of the simplest model systems where the interplay of quantum mechanical coherence and many-body effects can be studied, both in theory and experiment.

To set up the description, we first neglect interactions and imagine a single electron moving through the interferometer. The interferometer itself is described as two parallel 1D channels in which electrons propagate into the same direction (see figure 1(a)). At two tunnel contacts (i.e. QPCs in the experimental realization), these channels are coupled by tunneling amplitudes  $t_A$  and  $t_B$ . Further below, we will assume these tunneling probabilities to be small perturbations, coupling lead 1 (left channel) and lead 2 (right channel). Furthermore, a magnetic flux is enclosed by the interferometer, which leads to an additional Aharonov–Bohm phase  $\phi$ .

In the experiment the current  $I$  through the interferometer, i.e. the current between the two leads, measured at the output port, is the quantity of interest (see figure 1). It contains two types of contributions: one flux-independent constant term and one interference term that depends on  $\cos(\phi)$ . The contrast of the interference fringes observed in  $I(\phi) = I_0 + I_{\text{coh}}(\phi)$  can be quantified via the so-called visibility.

$$v_I = \frac{I_{\text{max}} - I_{\text{min}}}{I_{\text{max}} + I_{\text{min}}}, \quad (1)$$

where  $I_{\text{max}}$  ( $I_{\text{min}}$ ) are the maximum (minimum) current as a function of flux. This definition is chosen such that the visibility is equal to one for perfect interference contrast. This can be used as a direct measure for the coherence of the system. The coherence can be destroyed by the influence of an external bath as well as by internal interactions like the Coulomb interaction between the electrons inside the interferometer.

Treating the interferometer as a many-body system yields expressions for the current through the interferometer, which are not as obvious in a physical sense as in the single particle picture. Therefore the goal of this section is to formulate the quantities of interest in the physically most intuitive and transparent way.

### 2.1. Current

The observable of interest in the present setup is the current through the interferometer (see figure 1(a)) due to a finite bias voltage between the two leads, i.e.  $\mu_1 - \mu_2 \neq 0$ . Dealing with the electron–electron interaction exactly using the bosonization technique has the disadvantage that we have to treat the tunneling between the channels in perturbation theory. In the following, we define the QPCs A and B to be at the positions  $x_j^A = 0$  and  $x_j^B = x_j$ , respectively (where  $j = 1, 2$  is the channel index). Then the tunneling Hamiltonian is given by

$$\hat{H}^T := t_A \hat{\Psi}_1^\dagger(0) \hat{\Psi}_2(0) + t_B \hat{\Psi}_1^\dagger(x_1) \hat{\Psi}_2(x_2) + \text{h.c.} \quad (2)$$

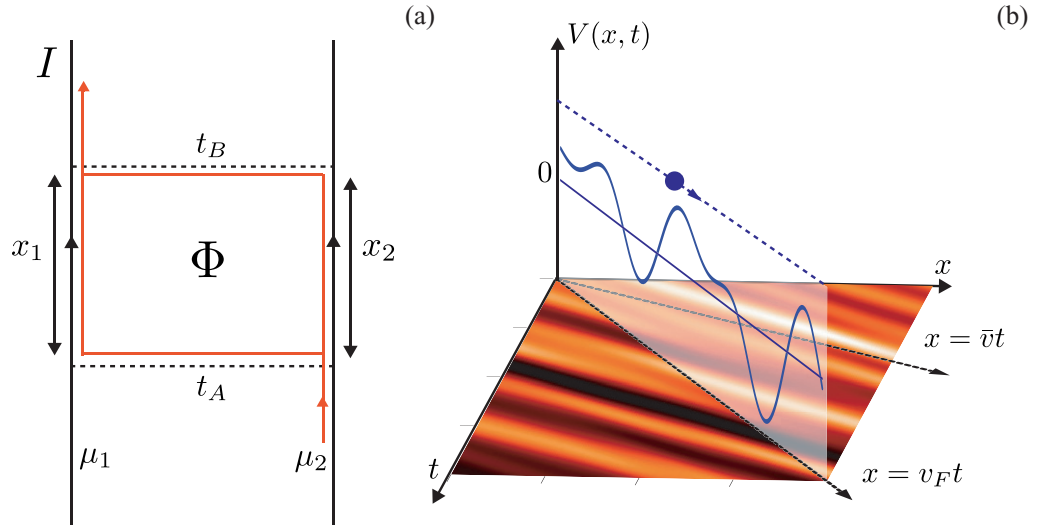


**Figure 1.** (a) Scheme of the interferometer setup. The two channels 1 and 2 of length  $x_{1,2}$  and the corresponding chemical potentials  $\mu_{1,2}$  are indicated. The electrons can tunnel at QPCs A and B, with tunnel amplitudes  $t_A$  and  $t_B$ . By tuning the magnetic flux  $\Phi$  through the interferometer, one observes an interference pattern  $I(\phi)$ . The solid orange lines denote the current through the interferometer. (b) A single electron propagating at high energies feels a fluctuating quantum potential  $\hat{V}(t)$ , due to the interaction with the density fluctuations in the sea of other electrons. We show a density plot of the potential, which is produced by the electronic density fluctuations (plasmons) in the channel. The plasmons are moving with a renormalized velocity  $\bar{v}$  (see main text) while the high-energy electron moves with the bare Fermi velocity  $v_F$ . It picks up a random phase, which leads to dephasing. This is the picture underlying the semiclassical approach in section 4.

The current into channel 1 is ( $q_e < 0$ ):

$$\hat{I} = q_e \frac{d}{dt} \hat{N}_1. \quad (3)$$

Thus the Heisenberg equation of motion yields

$$\hat{I} = -q_e i [\hat{N}_1, \hat{H}_0 + \hat{H}^T] = -q_e i \left[ t_A \hat{\Psi}_1^\dagger(0) \hat{\Psi}_2(0) + t_B \hat{\Psi}_1^\dagger(x_1) \hat{\Psi}_2(x_2) \right] + \text{h.c.} \quad (4)$$

Now we change to the interaction picture with respect to  $\hat{H}_0$  (where  $\hat{H}_0$  denotes the interacting electron Hamiltonian in the absence of tunneling, which we define in section 3), setting  $\hat{A}_{H_0}(t) \equiv e^{i\hat{H}_0 t} \hat{A} e^{-i\hat{H}_0 t}$ . We are interested in the steady-state current through the interferometer, which we obtain as a Kubo-type expression, in linear response with respect to the tunneling Hamiltonian, at arbitrary bias voltages:

$$I = \frac{1}{i} \int_{-\infty}^0 dt \left\langle \left[ \hat{I}_{H_0}(0), \hat{H}_{H_0}^T(t) \right] \right\rangle. \quad (5)$$

## 2.2. Evaluation of the current

Starting from equation (5) and plugging in the appropriate definitions an explicit expression for the current can be found. It will be convenient to express the current in terms of the unperturbed GFs of the chiral electron liquids in the two channels. These GFs will therefore be the primary object of our subsequent discussions.

2.2.1. *GFs.* In particular, we will analyze the particle- and hole-propagators

$$G^>(x, t) \equiv -i \left\langle \hat{\Psi}(x, t) \hat{\Psi}^\dagger(0, 0) \right\rangle, \quad (6)$$

$$G^<(x, t) \equiv +i \left\langle \hat{\Psi}^\dagger(0, 0) \hat{\Psi}(x, t) \right\rangle, \quad (7)$$

where we omit the channel index for brevity, unless needed for clarity. The Fourier transforms are obtained as  $G^>(k, \omega) = \int dx \int dt e^{-i(kx - \omega t)} G^>(x, t)$ . In addition, we will need the spectral density  $\mathcal{A}(k, \omega)$ ,

$$\mathcal{A}(k, \omega) \equiv -\frac{1}{\pi} \text{Im} [G^R(k, \omega)], \quad (8)$$

where  $G^R(x, t) = -i\Theta(t)\langle\{\hat{\Psi}(x, t), \hat{\Psi}^\dagger(0, 0)\}\rangle$ . The energy-dependent tunneling density of states follows as

$$\nu(\omega) := \int_{-\infty}^{\infty} dk \mathcal{A}(\omega, k). \quad (9)$$

2.2.2. *Flux-independent part of the current.* The flux-independent part of the current is found using equations (2), (4) and (5)

$$I_0 = q_e (|t_A|^2 + |t_B|^2) \int_{-\infty}^{\infty} dt [G_1^>(0, -t)G_2^<(0, t) - G_1^<(0, -t)G_2^>(0, t)], \quad (10)$$

which we rewrite by going to the frequency domain

$$I_0 = q_e (|t_A|^2 + |t_B|^2) \int (d\omega) [G_1^>(0, \omega)G_2^<(0, \omega) - G_1^<(0, \omega)G_2^>(0, \omega)], \quad (11)$$

where  $\int (d\omega) \dots = \int d\omega/2\pi \dots$ . Using the identities

$$G_j^>(x=0, \omega) = \int (dk) G_j^>(k, \omega) = -i [1 - f_j(\omega)] \nu_j(\omega), \quad (12)$$

$$G_j^<(x=0, \omega) = i f_j(\omega) \nu_j(\omega), \quad (13)$$

we can reformulate the expression as a function of the tunneling density of states  $\nu(\omega)$ ,

$$I_0 = q_e (|t_A|^2 + |t_B|^2) \int (d\omega) \nu_1(\omega) \nu_2(\omega) \left[ \underbrace{f_2(\omega)[1 - f_1(\omega)]}_{2 \rightarrow 1} - \underbrace{f_1(\omega)[1 - f_2(\omega)]}_{1 \rightarrow 2} \right],$$

where  $f_j(\omega)$  denotes the Fermi function, which finally yields the most intuitive form describing the sum of tunneling currents at two point-like locations:

$$I_0 = q_e (|t_A|^2 + |t_B|^2) \int (d\omega) v_1(\omega) v_2(\omega) [f_2(\omega) - f_1(\omega)]. \quad (14)$$

In particular, these expressions show that the flux-independent part of the current only depends on the tunneling density of states. It is independent of the length of the interferometer arms. This is to be expected, as that part of the current is insensitive to the electrons' coherence, and therefore the decay of coherence as a function of propagation distance will not enter here.

*2.2.3. Coherent part.* The Mach–Zehnder setup is intended to investigate the coherence of the electron system and therefore the most interesting quantity is the coherent part of the current, which we define to be the flux-dependent contribution. Again, using equations (2), (4) and (5) it yields:

$$I_{\text{coh}}(\phi) = q_e \int (d\omega) [(t_A t_B^*) e^{-i\phi} \cdot G_1^>(\omega, x_1) G_2^<(\omega, -x_2) - (t_A^* t_B) e^{i\phi} \cdot G_1^<(\omega, -x_1) G_2^>(\omega, x_2)] + \text{c.c.} \quad (15)$$

At  $T = 0$ , in a situation where the particle current flows from channel 2 to 1, only the first term (and its complex conjugate) contributes.

It might be helpful to see how the structure of this term  $G_1^> G_2^<$  can be understood in an intuitive, if slightly imprecise, way, that also relates to our subsequent semiclassical discussion. When the full beam in channel 2 impinges onto the first beam-splitter A, we obtain a superposition between two many-particle states: with an amplitude near unity, nothing happens (no tunneling takes place), and we denote this state as  $|0\rangle$ . There is a small chance (of amplitude  $t_A$ ) for a particle to tunnel through A into channel 1, leaving behind a hole in channel 2. As time passes, the second part acquires an amplitude (relative to the first) that is given by the product of propagation amplitudes for the electron ( $\psi_1$ ) and the hole ( $\psi_2^*$ ), resulting in:

$$|0\rangle + t_A \psi_1 \psi_2^* |1_p, 2_h\rangle. \quad (16)$$

Including the action of the second beam splitter B, and the Aharonov–Bohm phase, the total probability to detect an extra electron in the output port (channel 1) is therefore

$$|t_B e^{i\phi} + t_A \psi_1 \psi_2^*|^2, \quad (17)$$

which gives rise to the interference term

$$t_A t_B^* e^{-i\phi} \psi_1 \psi_2^* + \text{c.c.} \quad (18)$$

Averaging the amplitudes over phase fluctuations induced by the interaction, we arrive at the propagators, replacing  $\langle \psi_1 \rangle$  by the particle propagator  $G_1^>$ , and  $\langle \psi_2^* \rangle$  by the hole propagator  $G_2^<$ . The full analysis keeps track of energy conservation.

Thus, in the many-body picture, the observation of an interference term in the current is seen to depend both on the passage of an electron through channel 2 ( $G_2^>$ ) as well as the coherent propagation of the corresponding hole, of the same energy  $\omega$ , in channel 1 ( $G_1^<$ ). This issue has been discussed before, both for the Mach–Zehnder interferometer and weak localization [8, 10, 17, 21].

### 2.3. Visibility

In the Mach–Zehnder setup, the so called visibility is used as a measure of the coherence of the system. There are different definitions (experimentally, often the differential visibility is employed). However, we will define the visibility in terms of the total current, as

$$v_I(V, T) \equiv \frac{\max_{\phi} I_{\text{coh}}(\phi)}{I_0} = \frac{I_{\text{max}} - I_{\text{min}}}{I_{\text{max}} + I_{\text{min}}}. \quad (19)$$

The bias voltage is defined as  $\mu_1 - \mu_2 = q_e V$  and we set  $V > 0$ . We will also focus on zero temperature, as this seems to be the most interesting case. Now the visibility can be written in a compact form (here shown for  $T = 0$ ):

$$v_I = \frac{2|t_A t_B^*|}{|t_A|^2 + |t_B|^2} \cdot \frac{\left| \int_0^{|q_e V|} d\omega G^>(\omega, x_1) \cdot G^<(\omega - |q_e| V, -x_2) \right|}{\int_0^{|q_e V|} d\omega v(\omega) \cdot v(\omega - |q_e| V)}, \quad (V \geq 0). \quad (20)$$

Note that the channel indices of the GFs are omitted, as in this formula the GFs are defined with respect to a fixed density (and potential  $u_j = 0$ ) and all the explicit dependence on the bias voltage is shifted to the GF arguments.

Motivated by the structure of equation (15) in the following we will focus the attention on analyzing the function  $G_j^>(\epsilon, x)$  in three different ways. First we will apply the bosonization technique, i.e. we will include the intrinsic interaction in all orders. The main disadvantage of the bosonized picture is that we are looking at single particles tunneling between channels, while we are phrasing the description in terms of collective, bosonic excitations which prohibit a simple physical picture of the process of dephasing. Therefore, as an alternative point of view, we will discuss a transparent semiclassical model for electrons propagating high above the Fermi energy, subject to the fluctuations produced by the rest of the electrons. Finally, we will complement this analysis by studying the system in Keldysh perturbation theory for the fermions, up to second order in the coupling strength.

## 3. Solution by bosonization

In this section we recall how to obtain the GFs needed here via bosonization [37, 38]. Experienced readers may skip the section, and can refer to it later regarding the notation.

### 3.1. Hamiltonian and formal solution

We start from interacting right-moving chiral fermions in the two channels  $j = 1, 2$ , employing a linearized dispersion relation (we set  $\hbar = 1$ ):

$$\hat{H}_0 = \sum_{j=1,2} \left[ \sum_{k>0}^{\infty} (u_j + v_F k) \hat{c}_{j,k}^{\dagger} \hat{c}_{j,k} + \hat{H}_{\text{int},j} \right], \quad (21)$$

where  $v_F$  denotes the Fermi velocity and  $u_j$  is a constant which fixes the chemical potential of the channel. The particle operators for the chiral electrons are

$$\hat{\Psi}_j(x) = \frac{1}{\sqrt{L}} \sum_{k>0} e^{ikx} \hat{c}_{j,k}, \quad (22)$$

where  $L$  describes the size of the artificial normalization volume (with  $L \rightarrow \infty$  in the end). We also introduce the density fluctuations within each channel:

$$\hat{\rho}_j(x) \equiv \hat{\Psi}_j^\dagger(x)\hat{\Psi}_j(x) - \bar{\rho}_j \quad (23)$$

such that the Fourier components are given by

$$\hat{\rho}_j(x) = \frac{1}{L} \sum_{q \neq 0} \hat{\rho}_{q,j} e^{iqx}, \quad (24)$$

$$\hat{\rho}_{q,j} = \sum_{k>0} \hat{c}_{k,j}^\dagger \hat{c}_{k+q,j}, \quad (25)$$

with  $\hat{\rho}_{-q,j} = \hat{\rho}_{q,j}^\dagger$ . The average density  $\bar{\rho}_j$  enters  $\mu_j = u_j + 2\pi v_F \bar{\rho}_j$ .

As we take the two interferometer channels to be spatially separated, we only have to take care of intrachannel interactions. Transforming the interaction Hamiltonian

$$\hat{H}_{\text{int},j} = \frac{1}{2} \int dx \int dx' \hat{\Psi}_j^\dagger(x) \hat{\Psi}_j^\dagger(x') U(x-x') \hat{\Psi}_j(x') \hat{\Psi}_j(x) \quad (26)$$

into momentum space yields

$$\hat{H}_{\text{int},j} = \frac{1}{2L} \sum_{k>0, k'>0, q} U_q \hat{c}_{k+q,j}^\dagger \hat{c}_{k'-q,j}^\dagger \hat{c}_{k',j} \hat{c}_{k,j}, \quad (27)$$

where  $U_q = \int dx e^{-iqx} U(x)$  are the Fourier components of the interaction potential.

We construct bosonic operators from the Fourier components of the density in the standard way. As we are only dealing with chiral electrons, we only need to consider  $q > 0$  in the following:

$$(q > 0) \quad \hat{b}_{q,j} = \left(\frac{2\pi}{Lq}\right)^{1/2} \hat{\rho}_{q,j}, \quad \hat{b}_{q,j}^\dagger = \left(\frac{2\pi}{Lq}\right)^{1/2} \hat{\rho}_{-q,j}. \quad (28)$$

These operators fulfill

$$\left[ \hat{b}_{j,q}, \hat{b}_{j',q'}^\dagger \right] = \delta_{j,j'} \delta_{q,q'}. \quad (29)$$

As usual, the main advantage of bosonization consists in being able to write the kinetic part of the Hamiltonian as a quadratic form in boson operators:

$$\hat{H}_0 = \sum_{j=1,2} \left[ v_F \sum_{q>0} q \hat{b}_{q,j}^\dagger \hat{b}_{q,j} + \mu_j \hat{N}_j \right] + \text{const.}$$

The interaction part of the Hamiltonian reads:

$$\hat{H}_{\text{int},j} = \frac{1}{L} \sum_{q>0} U_q \hat{\rho}_{q,j}^\dagger \hat{\rho}_{q,j}. \quad (30)$$

Thus, the Hamiltonian is already in diagonal form,

$$\hat{H} = \sum_{j=1,2} \left[ \sum_{q>0} \omega(q) \hat{b}_{q,j}^\dagger \hat{b}_{q,j} + \mu_j \hat{N}_j \right] \quad (31)$$

with the plasmonic dispersion relation of an interacting chiral 1D electron system:

$$\omega(q) = v_F q \left[ 1 + \frac{U_q}{2\pi v_F} \right]. \quad (32)$$

For the following discussions, we introduce the dimensionless coupling constant  $\alpha = \frac{U(q \rightarrow 0)}{2\pi v_F}$ , where  $\alpha \in ]-1, \infty[$ . The renormalized plasmon velocity at small wavenumbers is  $\bar{v} = v_F(1 + \alpha)$ . Negative values of the coupling constant are related to attractive interactions, positive values to repulsion (at small wavenumbers). For  $\alpha \rightarrow -1$  the plasmon velocity tends to zero,  $\bar{v} \rightarrow 0$ . For  $\alpha < -1$  the system is unstable, i.e. formally  $\omega(q) < 0$  for  $q > 0$ .

The final step is to express the single-particle operators using bosonic fields [37, 38] (assuming  $L \rightarrow \infty$ ):

$$\hat{\Psi}_j(x) = \frac{\hat{F}_j}{\sqrt{2\pi a}} e^{ik_F x} e^{-i\hat{\Phi}_j(x)}, \quad \hat{\Phi}_j(x) = i \sum_{q>0} \sqrt{\frac{2\pi}{Lq}} e^{-aq} [\hat{b}_{q,j} e^{iqx} - \text{h.c.}]. \quad (33)$$

The ultraviolet cutoff length  $a$  is sent to zero at the end of the calculation. The Klein operator  $\hat{F}_j$  annihilates a fermion in a spatially homogeneous way, with the following commutation relations:

$$\{F_i, F_j^\dagger\} = \delta_{i,j}; \quad \{F_i, F_j\} = \{F_i^\dagger, F_j^\dagger\} = 0. \quad (34)$$

The explicit time dependence of the Klein operators is obtained by using the Heisenberg equation of motion, i.e.  $d\hat{F}_j/dt = -i[\hat{F}_j, \hat{H}] = -i\mu_j \hat{F}_j \Rightarrow \hat{F}_j(t) = e^{-i\mu_j t} \hat{F}_j(0)$ . In the end taking into account the relation  $k_{F,j} = \frac{2\pi}{L} \bar{N}_j$ , we arrive at

$$\hat{\Psi}_j(x) = \hat{F}_j \frac{1}{\sqrt{2\pi a}} e^{-i\mu_j(t-x/v_F)} \cdot e^{-i\hat{\Phi}_j(x,t)}. \quad (35)$$

### 3.2. GF from bosonization

Now we are able to evaluate the GF defined above explicitly using the bosonized single particle operators  $\hat{\Psi}$ . The calculation is done quickly using the fact, that the Hamiltonian in terms of the bosonic operators is quadratic, i.e. the field  $\hat{\Phi}[\hat{b}, \hat{b}^\dagger]$  can be treated like a Gaussian (quantum) variable, resulting in

$$G^>(x, t) = \frac{-i}{2\pi a} e^{-i\mu(t-x/v_F)} \exp \left[ \left\langle \hat{\Phi}(x, t) \hat{\Phi}(0, 0) \right\rangle - \left\langle \hat{\Phi}(0, 0)^2 \right\rangle \right], \quad (36)$$

and analogously for  $G^<$ . By factoring off the non-interacting GF  $G_0^{>/<}$ , we can write

$$G^{>/<}(x, t) = e^{-i\mu[t-x/v_F]} G_0^{>/<}(x, t) \exp[S_R(x, t) \mp iS_I(x, t)], \quad (37)$$

where

$$G_0^{>/<}(x, t) = \pm \frac{1}{2\beta v_F} \frac{1}{\sinh[\pi/\beta v_F](x - v_F t \pm i0^+)} \quad (38)$$

with  $\beta \equiv \frac{1}{T}$  and  $k_B \equiv 1$ . All the effects of the interaction now are included in the exponent where we have to subtract the non-interacting contribution:

$$S_R = \int_0^\infty \frac{dq}{q} \left\{ \underbrace{\coth[\beta\omega_q/2] [\cos[\omega_q t - qx] - 1]}_{\tilde{S}_R(\omega_q)} - \tilde{S}_R(\omega_q \rightarrow qv_F) \right\}, \quad (39)$$

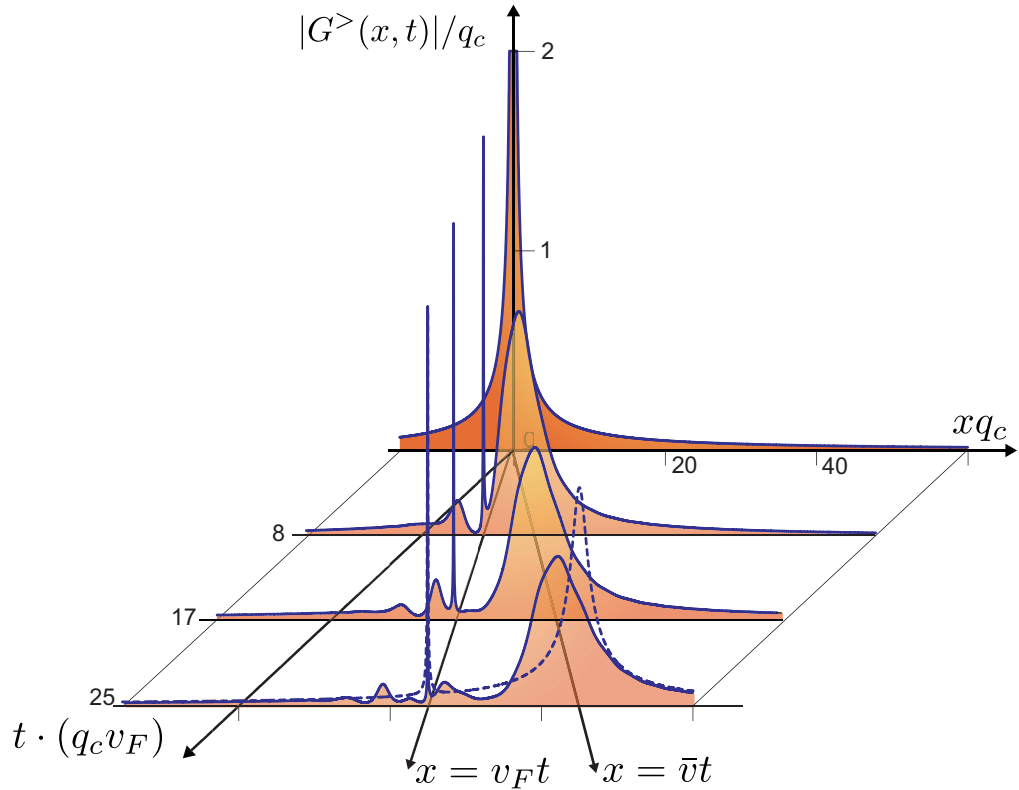


**Figure 2.** Numerical evaluation of  $|G^>(x, t)|$  at zero temperature  $T = 0$  resulting from bosonization, as a function of  $x$  and  $t$  (solid blue lines). The weight of the sharp peak at  $x = v_F t$  decreases for increasing propagation times  $t$ . The dashed blue line shows an approximation of the GF (see equation (42)) which yields good qualitative agreement with the full solution. The plot is done for  $U_q = U_0 e^{-(q/q_c)^2}$  with  $\frac{U_0}{v_F} = 2\pi\alpha = 5$ .

$$S_I = \int_0^\infty \frac{dq}{q} \left\{ \underbrace{\sin[\omega_q t - qx]}_{\tilde{S}_I(\omega_q)} - \tilde{S}_I(\omega_q \rightarrow q v_F) \right\}. \quad (40)$$

### 3.3. Discussion: GF in space and time

Here we discuss the GF as a function of space and time. A more detailed discussion can be found in [25]. The absolute value of the GF  $G^>(x, t)$  is shown in figure 2, at zero temperature (to which we restrict our discussion). In the following, all the numerical evaluations are performed using a generic smooth interaction potential  $U_q = U_0 e^{-(|q|/q_c)^s}$ . We note that all the qualitative results are valid for potentials which are finite at zero momentum ( $U_0 \neq 0$ ) and which are cut off beyond some momentum scale. Those assumptions are not restrictive and for example are fulfilled for a Coulomb potential with screening in a quasi 1D channel of finite width.

In figure 2, we observe as the main feature that the GF splits into two parts during its propagation. One of those propagates with the bare Fermi velocity  $v_F$  and represents the unperturbed GF, i.e. the high energy part. For increasing time its weight decreases, i.e. the

amplitude of the bare electron to arrive at  $x$  without being scattered decreases. The other peak represents the low energy part, stemming from energies below  $\epsilon - \mu \sim v_F q_c$ . It moves with the renormalized velocity  $\bar{v}$ .

We can obtain this structure of  $G^>(x, t)$  from a crude approximation. Namely for  $T = 0$  in a first approximation we can cut the momentum integral due to the fact that for  $q \gg q_c$  the integrand vanishes, i.e.

$$S[x, t] \equiv S_R - iS_I \approx \int_0^\infty \frac{dq}{q} e^{-q/q_c} [\exp[-iq(\bar{v}t - x)] - 1] - \int_0^\infty \frac{dq}{q} e^{-q/q_c} [\exp[-iq(v_F t - x)] - 1].$$

The integrals are known and yield

$$S[x, t] \approx \ln \left[ \frac{x - v_F t + iq_c^{-1}}{x - \bar{v}t + iq_c^{-1}} \right]. \quad (41)$$

Therefore, the structure of the GF is given by

$$G_{T=0}^>(x, t) \approx \frac{1}{x - v_F t + i0^+} \left[ \frac{x - v_F t + iq_c^{-1}}{x - \bar{v}t + iq_c^{-1}} \right], \quad (42)$$

displaying both the  $\delta$  peak at  $x = v_F t$  and the broadened peak at  $x = \bar{v}t$ , whose width is set by  $q_c^{-1}$ . In figure 2, one can observe the fairly good agreement between the full result and this first approximation.

### 3.4. GF versus position and energy

As shown above in equations (15) and (20), the current through the interferometer is determined by the propagators  $G^{> / <}(\epsilon, x)$ . Therefore, in the following our main focus will be on this function, which can be thought of as the amplitude for an electron of energy  $\epsilon$  to propagate unperturbed over a distance  $x$ .

The function is shown in figure 3, where we plot the numerical evaluation of the exact result obtained using the bosonization technique. This is done for two values of the coupling strength  $\alpha$  and for different interaction potentials. There are some main features which can be observed by having a brief look at figure 3, while for a detailed discussion we refer to the following section.

1. At  $x = 0$ , where  $|G^>(x = 0, \epsilon)| = v(\epsilon)$  equals the tunneling density of states, there is a finite dip at low energies. This is a static interaction effect. For repulsive interactions it represents the suppression of the tunneling density by a factor  $v_F/\bar{v}$ , due to the interaction-induced increase of the velocity  $\bar{v}$ . At high energies ( $\epsilon \gg v_F q_c$ ), the non-interacting density of states is recovered.
2. At any fixed energy  $\epsilon$ , the GF decays with increasing propagation length  $x$ . The shape of the decay (as a function of  $x$ ) becomes independent of energy for high energies. In contrast, the decay is suppressed for energies below  $\epsilon \sim v_F q_c$ , and there is no decay in the limit  $\epsilon \rightarrow 0$ . The decay of the GF is equivalent to dephasing (since in our model there are no interbranch interactions and correspondingly no vertex corrections). As a consequence, the absence of decay at zero energy will lead to perfect visibility at  $T = 0$ ,  $V \rightarrow 0$ .

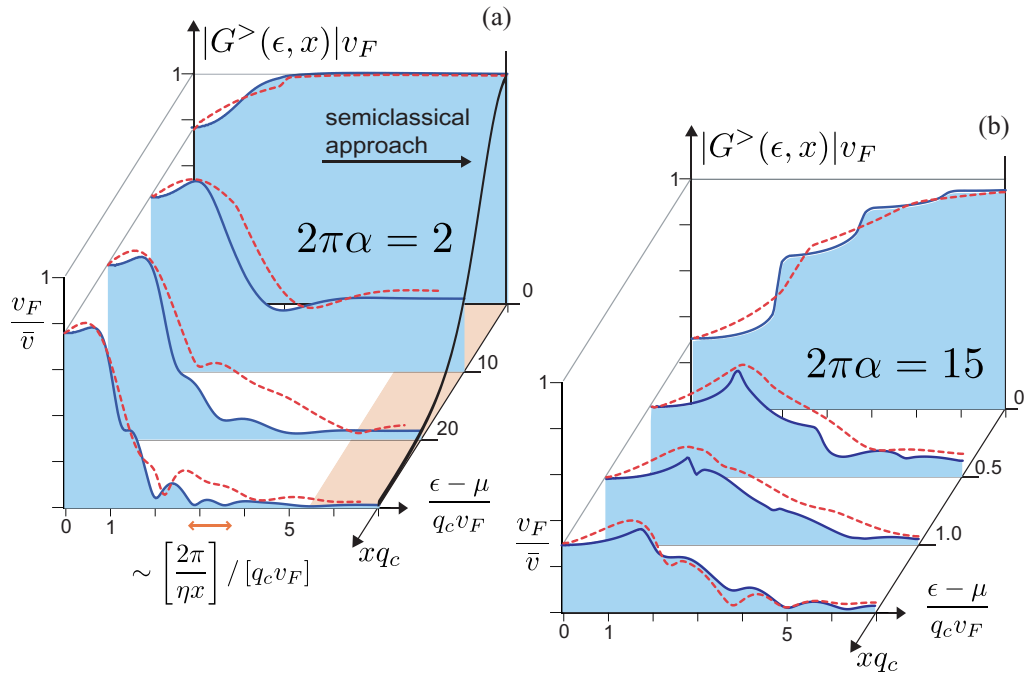


**Figure 3.** (a) The electron GF  $|G^>(x, \epsilon)|$ , for different lengths  $x$  as a function of energy  $\epsilon$ , evaluated using bosonization, for  $U(q) = U_0 e^{-(q/q_c)^2}$  (solid blue lines) and for  $U(q) = U_0 e^{-|q/q_c|}$  (dashed red lines). At high energies we show the result coming from the semiclassical approach for the Gaussian potential (solid black line). The red area indicates the regime of validity for the semiclassical (high-energy) approximation. The interaction strengths are:  $2\pi\alpha = 2$  (a) and  $2\pi\alpha = 15$  (b). In the high-energy limit, the semiclassical solution is valid for arbitrary coupling strength. However, the energies for which the description is valid become larger for increasing coupling strength. In (b) this limit is beyond the presented energy interval. Therefore, here we do not show the semiclassical solution.

- At larger  $x$ , there are oscillations in the GF. These result from the double-peak structure in the time-domain, with peaks at  $x = vt$  and  $x = \bar{v}t$ . These lead to a beating term  $\exp[i\omega x(v^{-1} - \bar{v}^{-1})]$  in  $|G^>(x, \omega)|$ . Therefore, the period of oscillations in the energy domain is determined by the difference between the bare and the renormalized velocity (see figure 3), viz.:

$$\delta\epsilon \approx \frac{2\pi}{x\eta}; \quad \text{with } \eta = \frac{1}{v} - \frac{1}{\bar{v}}. \quad (43)$$

### 3.5. Large coupling constants

In this section, we want to discuss briefly the shape of the GF in terms of the coupling strength. We emphasize that, once the shape of the interaction potential is given, the only dimensionless parameter left is the coupling constant  $\alpha = U_0/(2\pi v_F)$ . All the other parameters may be absorbed into a rescaling of the result.

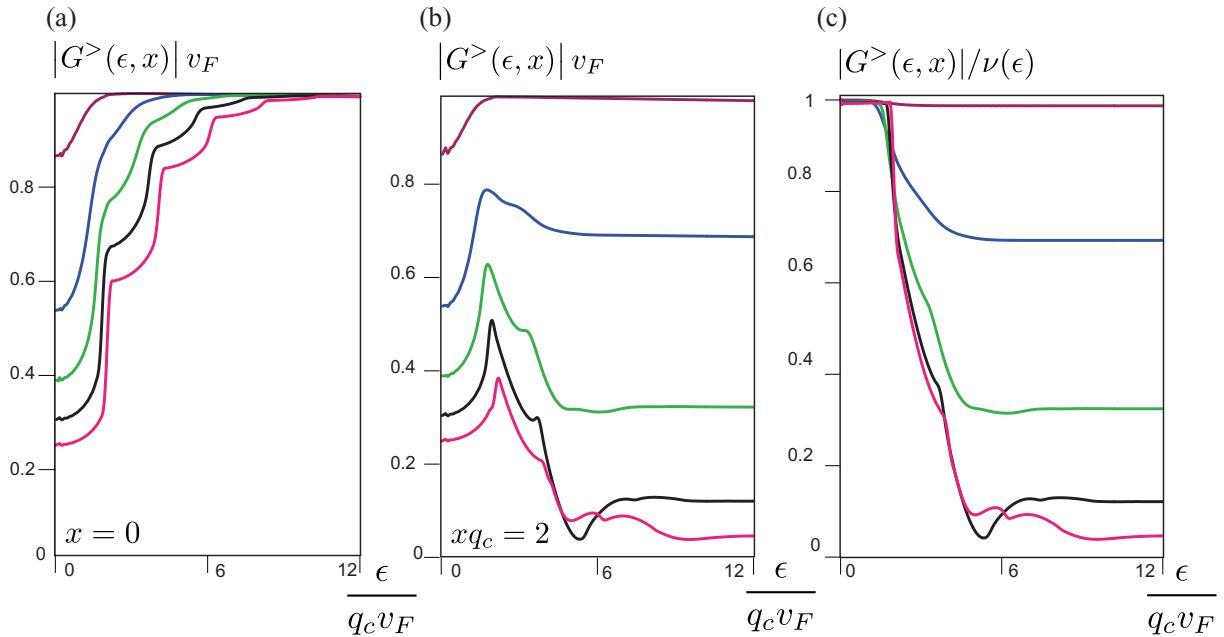


**Figure 4.** GF at zero temperature  $T = 0$  as a function of energy  $\epsilon$  for various coupling strengths  $\alpha$ , at  $x = 0$  (a) and  $x q_c = 2$  (b). (c)  $|G^>(\epsilon, x)|$  for  $x q_c = 2$ , divided by the tunnel density of states  $\nu(\epsilon) = |G^>(\epsilon, x = 0)|$ . This might be interpreted as the electron's coherence as a function of propagation energy and distance. Here, the potential is  $U_q = 2\pi\alpha v_F e^{-(q/q_c)^2}$ , where the various values of  $\alpha$  are (from top to bottom):  $\alpha = 0.16, 0.9, 1.6, 2.3, 3$ .

In figure 4, we show  $|G^>(\epsilon, x)|$  as a function of energy for various coupling strengths (different curves), both at  $x = 0$  and at some finite propagation distance  $x \neq 0$ . For small coupling  $\alpha > 0$ , we just observe the suppression of the tunneling density of states discussed above. Upon increasing the coupling strength, a series of rounded steps emerges, suppressing the tunneling density even further. The same features can be seen in the shape of the GF at finite  $x$ , though there they are superimposed by the decay (describing decoherence) and the oscillations as a function of energy (discussed in the preceding section). To identify the oscillations in energy which we observe even for small coupling strength in figure 4(c) we divide the GF for  $x \neq 0$  showed in figure 4(b) by the tunnel density of states. As expected, those oscillations are robust against a change in the coupling strength. We have not found any simple analytical model to discuss the structures observed here. However, note that in figure 3(b) one observes that the step structure is more pronounced for the Gaussian potential compared to the results for the exponential shape. That shows the strong influence of the shape of the interaction potential on the step structure.

We note that the previous discussion in the  $(\epsilon, k)$ -space (as opposed to  $(\epsilon, x)$ ) had found non-analytic structures for the case of a box-shape potential  $U_q$  [34].

#### 4. Semiclassical model of dephasing

Up to now we have applied the bosonization technique in order to get exact information about the decoherence the electron suffers while passing through the interferometer. However, we

actually do not know what is going on in more physical terms. First of all, we do not know in detail how to distinguish between the single electron we are considering while traveling through the interferometer and the bath electrons which are present at the same time. In a Fermi liquid there is no question about the nature of the single electron, i.e. in the vicinity of the Fermi edge it can be described as a quasiparticle. In contrast, in the bosonization approach everything is described in terms of collective bosonic excitations, i.e. density fluctuations. Therefore, as soon as the electron tunnels into the interacting system, there is no way to trace this special electron any longer. This fact leads to difficulties in understanding the decoherence intuitively, since in the moment of tunneling the coherent phase information is encoded into the bosonic degrees of freedom. Fortunately, it turns out that indeed it is possible to find simple physical pictures which are helpful in understanding the process of dephasing in more detail besides the mathematical solution.

For energies much higher than the Fermi energy (to be made more precise below), it turns out that it is possible to describe the interaction of a single propagating electron with all the other electrons, by viewing them as a bosonic quantum bath. To see this, in section 4 we apply an intuitive, semiclassical method which is able to reproduce exactly the results from the full bosonization formalism in the high energy limit.

In a recent work [36], we have already briefly reported on universal dephasing for high-energy electrons at long distances for  $T = 0$ , based on the semiclassical approach to be discussed in more detail in the following.

#### 4.1. Semiclassical approach to the GF

Electrons at high energies  $\epsilon$  propagate at the unperturbed speed  $v_F$ , as can be observed from the corresponding limiting behavior of the plasmonic dispersion relation. The decoherence, i.e. the GF, can be described in a transparent semiclassical framework, that becomes exact in the limit of high energies. We will confirm this later by comparing against the full bosonization solution. Within this semiclassical picture, one thinks of the electron propagating through the channel, while accumulating an additional phase due to the interaction with the bath formed by all the other electrons. To model the effective, bosonic bath acting on the single electron, we make use of the plasmonic dispersion relation which was derived using the full bosonization technique (equation (32)). As the electron we consider is flying high above the Fermi sea, we can neglect the back action of the electron onto the bath. In this picture the electron only experiences the intrinsic fluctuations of the bath. The potential acting on such a single high-energy electron is obtained by convoluting the density fluctuations with the interaction potential:

$$\hat{V}(t) = \int dx' U(x' - v_F t) \hat{\rho}(x', t). \quad (44)$$

Note that this definition implies that the effective potential fluctuations  $\hat{V}(t)$  experienced by the single electron are just the fluctuations of the bath evaluated at the classical electron position  $x = v_F t$  at time  $t$ . This is why we call this model ‘semiclassical’.

If we were dealing with a classical fluctuating potential  $V(t)$ , the electron would simply pick up a random phase  $\varphi(t) = -\int_0^t dt' V(t')$ . In that case the non-interacting GF would have to be multiplied by a factor  $\langle e^{i\varphi(t)} \rangle$  to obtain the correct GF. However, if the quantum nature of the bath becomes important one has to take care of the non-commutativity of the operator  $\hat{V}(t)$

at different times. This can be done by introducing a time-ordering symbol:

$$\begin{aligned} e^{-F(t)} &\equiv \left\langle \hat{T} \exp \left[ -i \int_0^t dt' \hat{V}(t') \right] \right\rangle \\ &= \exp \left[ -\frac{1}{2} \int_0^t dt_1 \int_0^t dt_2 \left\langle \hat{T} \hat{V}(t_1) \hat{V}(t_2) \right\rangle \right]. \end{aligned} \quad (45)$$

The time  $t = x/v_F$  in equation (45) is determined by the propagation length. This is actually identical to the decay of coherence of a single level whose energy fluctuates. In various contexts, this is known as the ‘independent boson model’ [39, 40], or the case of ‘pure dephasing’ in a (longitudinally coupled) spin-boson model [1].

We note that the same kind of approach to dephasing of ballistically propagating electrons has been introduced previously, both for a situation with a general quantum bath [10, 17, 21], as well as for two coupled Luttinger liquids [30].

Furthermore, we note that the decay is independent of energy  $\epsilon$ . This is because the propagation speed is energy-independent, and the distance to the Fermi edge becomes unimportant at high energies as well. Qualitatively, we have seen this feature before in our discussion of the full bosonization solution.

In summary, the decay of coherence, described by  $F(t)$ , is completely determined by the fluctuation spectrum  $\langle \hat{V} \hat{V} \rangle_\omega = \int dt e^{i\omega t} \langle \hat{V}(t) \hat{V}(0) \rangle$  of the potential seen by the electron in the moving frame. To proceed further we express the time-ordered correlator  $\langle \hat{T} \hat{V}(t_1) \hat{V}(t_2) \rangle$  as a sum of commutator and anti-commutator part:

$$\langle \hat{T} \hat{V}(t_1) \hat{V}(t_2) \rangle = \frac{1}{2} \left[ \left\langle \left\{ \hat{V}(t_1), \hat{V}(t_2) \right\} \right\rangle + \text{sgn}(t_1 - t_2) \left\langle \left[ \hat{V}(t_1), \hat{V}(t_2) \right] \right\rangle \right]. \quad (46)$$

The real part of  $F(t)$  and therefore the decay of the GF depends on the symmetrized part of the correlator. This part is formally similar to the correlator of classical noise, though it also contains the zero-point fluctuations of the plasmon field:

$$\text{Re}[F(t)] = \frac{1}{4} \int_0^t dt_1 \int_0^t dt_2 \left\langle \left\{ \hat{V}(t_1), \hat{V}(t_2) \right\} \right\rangle = \int_{-\infty}^{+\infty} \frac{d\omega}{2\pi} \frac{\sin^2(\omega x/2v_F)}{\omega^2} \left\langle \left\{ \hat{V}, \hat{V} \right\} \right\rangle_\omega. \quad (47)$$

In addition, a phase  $-\text{Im}F(t)$  shows up in the exponent. It is due to the commutator of  $\hat{V}$ , and thus it represents a purely quantum mechanical contribution. In terms of the Fourier transform of the spectrum, this yields

$$\begin{aligned} \text{Im}[F(t)] &= -\frac{i}{4} \int_0^t dt_1 \int_0^t dt_2 \text{sgn}(t_1 - t_2) \left\langle \left[ \hat{V}(t_1), \hat{V}(t_2) \right] \right\rangle \\ &= -\frac{1}{2} \int_{-\infty}^{+\infty} \frac{d\omega}{2\pi} \left[ \frac{t}{\omega} - \frac{\sin(\omega t)}{\omega^2} \right] \left\langle \left[ \hat{V}, \hat{V} \right] \right\rangle_\omega. \end{aligned} \quad (48)$$

From equation (44), we obtain for the potential spectrum in the co-moving frame

$$\left\langle \hat{V} \hat{V} \right\rangle_\omega = \int \frac{dq}{2\pi} |U_q|^2 \langle \hat{\rho} \hat{\rho} \rangle_{q, \omega + v_F q}. \quad (49)$$

The argument  $\omega + v_F q$  indicates that we are dealing with the Galileo-transformed spectrum of the density fluctuations. As a result, the spectrum of the density fluctuations gets tilted compared to the original dispersion relation (see figure 5). Making use of the plasmonic dispersion  $\omega(q)$ , which we obtained from the bosonization method, the density–density correlator yields

$$\left\langle \hat{\rho} \hat{\rho} \right\rangle_{q, \omega} = \frac{|q|}{1 - e^{-\beta\omega}} \cdot [\Theta(q)\delta(\omega - \omega(|q|)) - \Theta(-q)\delta(\omega + \omega(|q|))]. \quad (50)$$

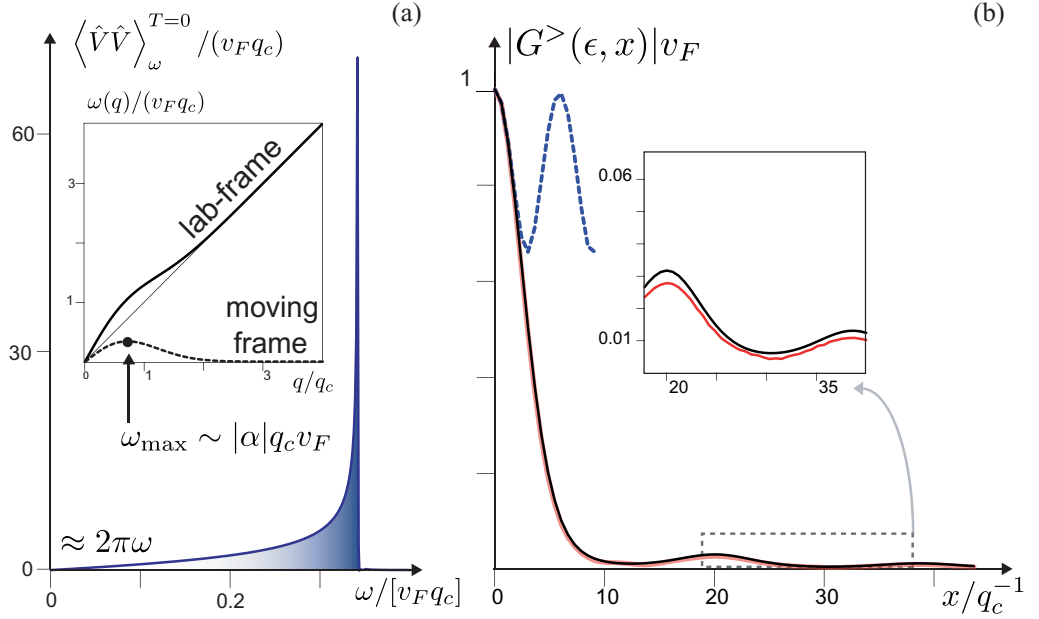


**Figure 5.** (a) Plot of the effective spectrum  $\langle \hat{V} \hat{V} \rangle_{\omega}^{T=0}$  (here for  $\alpha > 0$ ) of the plasmonic bath at the particle position which moves with velocity  $v_F$ . The spectrum is linear in  $\omega$  for small frequencies and diverges like  $\frac{1}{\sqrt{\omega_{\max} - \omega}}$  when approaching  $\omega_{\max}$ . The inset shows the dispersion relation of the plasmonic bath in the laboratory frame of reference as well as in the electron frame of reference, where it is getting tilted (dashed curve). (b)  $G^>(\epsilon, x)$  as a function of  $x$  for large energies  $\epsilon \gg q_c v_F$ . The solid orange line denotes the numerical evaluation of the bosonization result, while the solid black line shows the semiclassical result. For a better comparison of the results, the inset shows a blow-up of the oscillations. The small deviations are due to finite numerical precision. In addition, the dashed line denotes the solution of the Keldysh perturbation theory. All the plots are done for  $U_q = U_0 e^{-(q/q_c)^2}$  with  $\frac{U_0}{v_F} = 2\pi\alpha = 5$ .

We obtain

$$\langle [\hat{V}, \hat{V}] \rangle_{\omega} = \int \frac{dq}{2\pi} |U_q|^2 \langle [\hat{\rho}, \hat{\rho}] \rangle_{q, \omega + qv_F}, \quad (51)$$

$$\langle \{ \hat{V}, \hat{V} \} \rangle_{\omega} = \int \frac{dq}{2\pi} |U_q|^2 \coth \left( \frac{\beta(\omega + qv_F)}{2} \right) \langle [\hat{\rho}, \hat{\rho}] \rangle_{q, \omega + qv_F}. \quad (52)$$

The symmetrized correlator can be written as

$$\omega > 0: \quad \langle \{ \hat{V}, \hat{V} \} \rangle_{\omega} = \int_0^{\infty} \frac{dq}{2\pi} |U_q|^2 q \coth \left( \frac{\beta\omega(q)}{2} \right) \delta \left( \omega - \frac{|U_q q|}{2\pi} \right). \quad (53)$$

Plugging in these correlators in equations (47) and (48), finally yields  $F(t)$ :

$$\text{Re}[F(t)] = \int_0^{\infty} \frac{dq}{q} \coth \left( \frac{\beta\omega(q)}{2} \right) \left[ 1 - \cos \left( \frac{U_q q}{2\pi} t \right) \right]. \quad (54)$$

$$\text{Im}[F(t)] = \int_0^\infty \frac{dq}{q} \sin\left(\frac{U_q q}{2\pi} t\right) - \int_0^\infty dq \frac{U_q}{2\pi} t. \quad (55)$$

Indeed, up to an additional energy renormalization  $-\int_0^\infty dq \frac{U_q}{2\pi}$ , the resulting GF  $G^>(x = v_F t, t) = e^{-F(t)} G_0^>(x = v_F t, t)$  is identical to the one stemming from the bosonization technique for  $x = v_F t$  (compare to equations (39) and (40)). This constant energy shift had been incorporated into a redefinition of the chemical potential, as noted in the section on bosonization.

To be precise, equations (54) and (55) show that the decoherence of electrons moving along the trajectory  $x = v_F t$  can be described exactly in terms of the semiclassical approach (which is based on the assumption of high-energetic electrons). In order to prove the statement that the decoherence at large energies can be understood within the semiclassical description, one has to confirm the initial assumption that high energetic electrons actually move with the bare Fermi velocity  $v_F$ . Already, in section 3.3 we observed that the GF  $G^>(x, t = \frac{x}{v_F})$  determines the high-energy regime of the Fourier transform  $G^>(x, \epsilon)$ . This followed from the analysis of the GF  $G^>(x, t)$ . Beside a broad peak moving with  $\bar{v}$ , one observes a sharp peak in time, moving along the trajectory  $x = v_F t$ , which is obviously responsible for the contributions to  $G^>(\epsilon, x)$  at large energies. In addition, we confirm the assumption numerically. As we are not able to perform the Fourier transformation analytically, instead figure 5 shows the numerical evaluation of the function  $e^{-F(x)}$  and the direct Fourier transform of the GF  $G^>(x, t)$  resulting from the bosonization in the limit  $\epsilon \rightarrow \infty$ . Obviously, those turn out to be identical. Therefore we conclude that the semiclassical approach is becoming exact in the limit of high-energy electrons. We emphasize that, apart from the transparent interpretation of the decoherence of high energetic electrons via the semiclassical method, even the observation that the Fourier transform of the GF at high energies turns out to be identical to the  $[G^>(x, t)/G_0^>(x, t)]G_0^>(\epsilon, x)$  with  $x = v_F t$  is non-trivial and serves as a starting point for the analytical discussion of the decoherence in this regime.

Having established the connection between the semiclassical approach and the full bosonization solution, we now turn to the properties of the symmetrized potential spectrum. For this, first we focus on the zero temperature case  $T = 0$  (see figure 5). At high frequencies, we obtain a singularity  $\{\{\hat{V}, \hat{V}\}\}_\omega^{T=0} \propto 1/\sqrt{\omega_{\max} - |\omega|}$  at the cutoff frequency  $\omega_{\max} = \max(\omega(q) - v_F q)$ , which is the maximum frequency in the Galilei-transformed plasmon dispersion relation. Such a maximum frequency arises due to the momentum cutoff in the dispersion relation (which results from the finite range of the interactions). Due to this smooth momentum cutoff, the velocity of plasmons in the limit of large momenta is identical to the Fermi velocity  $v_F$  of the electron. By transforming the potential to the moving frame, it gets tilted (see figure 5). As the velocity of the plasmons in the limit of large momenta is identical to the velocity of the moving frame, the effective dispersion relation shows a maximum. The singularity in the spectrum arises due to the fact that  $\omega(q) \approx \omega_{\max} + \omega''(q - q^*)^2/2$  in the vicinity of  $q^*$ , where  $\omega(q^*) = \omega_{\max}$ . Note that an interaction potential  $U_q$  with a non-monotonous decay in  $q$  may give rise to several such singularities, corresponding to the local maxima of  $\omega(q) - v_F q$ .

At low frequencies  $\omega \ll v_F q_c$ , the spectrum increases linearly in  $\omega$ , corresponding to ‘Ohmic’ noise, which is ubiquitous in various other physical contexts [1]. For interaction potentials that are smooth in real space (i.e. where all the moments of  $|U_q|$  are finite), we find that the leading low-frequency behavior is determined solely by the contribution to equation (49)

stemming from small  $q$ . The result is (at any fixed  $\alpha \neq 0$ ):

$$\left\langle \{\hat{V}, \hat{V}\} \right\rangle_{\omega}^{T=0} = \frac{U_{q \rightarrow 0}^2}{(\bar{v} - v_F)^2} \frac{|\omega|}{2\pi} = 2\pi |\omega|. \quad (56)$$

Most remarkably, the dimensionless prefactor (the slope) of the noise spectrum turns out to be completely independent of the coupling strength  $\alpha$ , which drops out. This is in contrast to the typically studied non-chiral Luttinger liquids, where an Ohmic spectrum has been found with an interaction-dependent prefactor [30]. As a direct consequence, the electron's GF shows a universal power-law decay at long distances, as we will discuss in more detail in the next section.

#### 4.2. Universal dephasing for high-energy electrons

We insert (56) into the long-distance limit of equation (47):

$$\begin{aligned} \text{Re}[F(x)] &= 2 \lim_{x \rightarrow \infty} \int_0^{+\infty} \frac{d\omega}{2\pi} \frac{\sin^2(\omega x/2v_F)}{\omega^2} \left\langle \{\hat{V}, \hat{V}\} \right\rangle_{\omega}^{T=0} \\ &\approx \text{const} + \underbrace{\int_{v_F/x}^{\omega_c} d\omega \frac{1}{\omega}}_{\ln(x\omega_c/v_F)} + 2 \int_{\omega_c}^{\omega_{\max}} \frac{d\omega}{2\pi} \frac{\sin^2(\omega x/2v_F)}{\omega^2} \left\langle \{\hat{V}, \hat{V}\} \right\rangle_{\omega}^{T=0}, \end{aligned} \quad (57)$$

where the choice of  $\omega_c \ll \omega_{\max}$  is arbitrary (but related to the constant), and  $|G^>(\epsilon \rightarrow \infty, x)|_{v_F} = e^{-\text{Re}[F(x)]}$ . As a consequence of the logarithmic contribution to the exponent, the leading asymptotic behavior of the GF is a power-law decay with an interaction-independent exponent 1:

$$|G^>(\epsilon, x)| \propto \frac{1}{x}. \quad (58)$$

We recall the fact that equation (58) refers to the GF in energy-coordinate space, as a function of propagation distance  $x$  at large energies. Having shown previously that the current and thus the visibility only depend on this function (see equations (15) and (20)), we may denote it the ‘coherence’ of the electron. Therefore, equation (58) shows that the coherence itself displays a universal power-law decay. Please observe that in the absence of interactions  $|G^>(\epsilon, x)|$  would be constant, so the decay indeed implies interaction-induced decoherence. The surprising feature is the independence of the exponent from the strength of the interactions (while the prefactor, not displayed here, would indeed depend on the details of the potential).

In writing down equation (57), we have neglected the contributions of large momenta in equation (49). These will lead to a subleading correction to the power-law, which we discuss below. The third term in equation (57) is responsible for oscillations in the coherence  $|G^>(\epsilon, x)|$ , on top of the decay (see below). Figure 6 shows the decay of  $G^>(\epsilon \rightarrow \infty, x)$  for different coupling constants  $\alpha$ .

In order to understand how this generic result for the asymptotic decay is compatible with the non-interacting limit ( $\alpha = 0$ , where  $|G^>(\epsilon, x)|$  is constant), we have to discuss the range of validity of the asymptotic behavior. As the linear slope in the effective spectrum  $\langle \{\hat{V}, \hat{V}\} \rangle_{\omega}$  applies only at  $|\omega| \ll \omega_{\max}$ , we must certainly require  $\omega_{\max} x/v_F \gg 1$ . Since  $\omega_{\max}$  vanishes linearly with  $\alpha$ , the limiting regime is reached at ever larger values of  $x$  when the interaction strength is reduced. This shift of the range of validity is shown in figure 6.

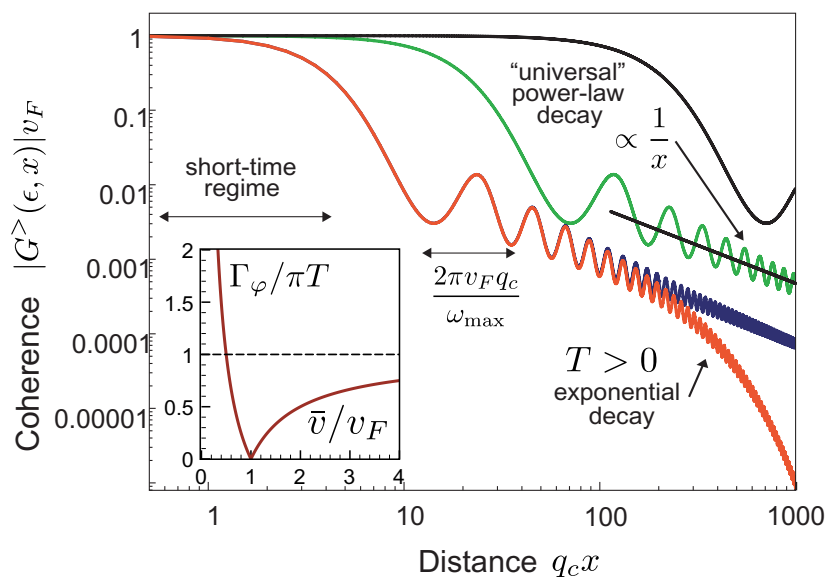


**Figure 6.** Coherence of an electron propagating at high energies in an interacting chiral system, as a function of propagation distance for various values of interaction strength  $\alpha$ :  $2\pi\alpha = 0.1$  (solid black line),  $2\pi\alpha = 1.0$  (solid green line) and  $2\pi\alpha = 5.0$  (solid red and blue). The potential is taken as  $U_q = U_0 e^{-|q/q_c|}$  and temperature is zero except for the red line where  $T/q_c v_F = 0.005$ . The non-interacting case would give  $v_F |G^>(\epsilon, x)| \equiv 1$ . The long-distance decay is universally given by  $\propto 1/x$ , independent of interaction strength. Note that for decreasing coupling strength the asymptotic power-law decay sets in for increasingly larger propagation distances. At finite temperatures, this power-law decay turns into an exponential decay for large  $x$  with a decay rate  $\Gamma_\varphi$  depending on interaction strength (inset).

The oscillatory modulation is due to the square root singularity at  $\omega \rightarrow \omega_{\max}$  in the spectrum  $\langle \hat{V} \hat{V} \rangle_\omega$ . Its amplitude depends on the interaction strength  $|\alpha|$  but vanishes at long distances (see appendix A.1):

$$F(x) \approx \text{const} + \ln(\omega_c x / v_F) - C \frac{\sin(\omega_{\max} x / v_F + \pi/4)}{\sqrt{2\pi} |\alpha| q_c x}, \quad (59)$$

where  $C$  is a numerical constant, which solely depends on the explicit form of the potential.

We now discuss the deviations from the leading low-frequency behavior of  $\langle \{\hat{V}, \hat{V}\} \rangle_\omega$ . Taking into account the contributions resulting from large  $q$  in equation (49), for smooth potentials like  $U_q = U_0 e^{-(|q|/q_c)^s}$  the correction is  $\langle \{\hat{V}, \hat{V}\} \rangle_\omega^{\text{sub}} = 2\pi\omega / (s \ln(|\alpha| v_F q_c / \omega))$  (A.2). In real space this expression translates into a correction  $\frac{1}{s} \ln(\ln(|\alpha| q_c x))$  to the decay function  $F(t = x/v_F)$  (A.3).

At finite temperature  $T \neq 0$ , the long-time limit is given by an exponential decay  $|G^>(x, \epsilon)| \propto \exp[-\Gamma_\varphi x / v_F]$ , with a decay rate

$$\Gamma_\varphi = \pi T \left| 1 - \frac{v_F}{\bar{v}} \right| = \pi T |1 + \alpha^{-1}|^{-1}. \quad (60)$$

This follows from the long-time limit of equation (47) together with equation (53):

$$\text{Re}[F(x)] \approx 2 \int_0^\infty dq \frac{\sin^2(q|U_q|x/(4\pi v_F)})}{q} \coth\left(\frac{|\omega(q \rightarrow 0)|}{2T}\right). \quad (61)$$

Using the identity  $\lim_{a \rightarrow \infty} \frac{\sin^2(ax)}{ax^2} = \pi \delta(x)$ , we get  $\text{Re}[F(x)] = \pi T |1 + \alpha^{-1}|^{-1} x$ , from which we obtain the aforementioned decay rate  $\Gamma_\varphi$ . In figure 6, the decay rate is shown as a function of the coupling  $\alpha$ . For small  $\alpha$ , this rate vanishes as  $\Gamma_\varphi = \pi T |\alpha|$ , i.e. it is non-analytic in  $U_0 \propto \alpha$ . Such dephasing rates proportional to  $T$  have also been found in non-chiral Luttinger liquids [31]–[32]. At large repulsive coupling,  $U_0 \rightarrow +\infty$ , we have the universal result  $\Gamma_\varphi \rightarrow \pi T$ . For attractive interaction,  $\Gamma_\varphi$  diverges upon approaching the instability at  $\alpha \rightarrow -1$ , where  $\bar{v} \rightarrow 0$  and where the resulting low-frequency modes are thermally strongly excited.

We note that this behavior is somewhat surprising when compared to other problems of dephasing. When considering pure dephasing of a two-level system by an Ohmic bath, a power-law decay  $t^{-\gamma}$  at  $T = 0$ , with an exponent  $\gamma$  set by the coupling, automatically implies an exponential decay at a rate  $\Gamma_\varphi = \pi \gamma T$  at finite temperatures. This follows from the fluctuation-dissipation theorem (FDT) which turns the  $T = 0$  Ohmic spectrum into a white-noise spectrum with a weight proportional to  $T$ .

However, in the present case, we have to take into account the Galileo transformation, which turns the laboratory-frame temperature  $T$  into an effective temperature  $T_{\text{eff}}$  in the frame moving along with the particle at speed  $v_F$ . In order to establish the FDT for the effective potential fluctuations in the electron frame of reference we therefore have to define the effective temperature  $T_{\text{eff}}$  by demanding for  $\omega \downarrow 0$

$$\begin{aligned} \langle \{ \hat{V}, \hat{V} \} \rangle_\omega &= \int_0^\infty \frac{dq}{2\pi} q |U_q|^2 \coth\left(\frac{\omega(q)}{2T}\right) \delta\left(\omega - \frac{|U_q q|}{2\pi}\right) \\ &\equiv \coth\left(\frac{\omega}{2T_{\text{eff}}}\right) \langle [ \hat{V}, \hat{V} ] \rangle_\omega. \end{aligned} \quad (62)$$

In the low-frequency limit we get  $\langle \{ \hat{V}, \hat{V} \} \rangle_\omega = 2\pi \omega \coth(\omega |1 + \alpha^{-1}| / (2T))$ . Together with equation (51), this yields the effective temperature  $T_{\text{eff}} \equiv T |1 + \alpha^{-1}|^{-1}$ . In the moving frame the frequencies are reduced by  $q_c v_F$  and therefore the effective temperature is also smaller. Only for large repulsive interactions ( $\bar{v} \gg v_F$ ), the transformation does not matter. Therefore, in this limit  $T_{\text{eff}} = T$  and the universal, coupling-independent power-law for  $T = 0$  turns into a universal decay rate at finite temperatures.

Finally, turn briefly to the question of observing these features in experiments. We note that the universal power-law decay of the GF should be observable in principle in the Mach–Zehnder interferometer setup, as it directly translates into a decay of the visibility itself. To obtain a numerical estimate, we assume a screened Coulomb potential with screening length  $q_c^{-1} \sim 10^{-7} \text{m}$  and a finite channel width  $b \sim 10^{-7} \text{m}$ . Following [25] the edge state velocity can be assumed to be:  $v_F \sim (10^4 - 10^5) \text{m s}^{-1}$ . Then the dimensionless coupling constant  $\alpha$  is of the order 1. To reach the high energy limit, the applied bias voltage  $V$  has to fulfill:  $q_e V \gg q_c v_F$ . For  $v_F = 10^4 \text{m s}^{-1}$ , it turns out that one has to apply  $V \sim 10^2 \mu\text{V}$  which is in the range of the bias voltages typically applied in experiments (in [12]  $V \sim 10^1 \mu\text{V}$ ). We mention that the long-distance limit should be reached for  $x \gg v_F / \omega_{\text{max}} \sim 10^{-1} \mu\text{m}$ , which is shorter than the typical interferometer arm length (e.g. in [12]  $x_{1,2} \sim 10^1 \mu\text{m}$ ). Thus there is some hope that the high-energy as well as the long-distance limit is accessible in the experiment. However, we note that the magnitude of the GF  $G^>(\epsilon, x)$  gets suppressed strongly when reaching the long-distance

limit, i.e.  $x \gg v_F/\omega_{\max}$ . For  $\alpha = 1$ , the magnitude of  $|G^>(\epsilon, x)|$  yields:  $|G^>(\epsilon, x)| \sim 10^{-2}$  (see figure 6). With help of equation (20) this translates into a visibility of the order  $v_I \sim 10^{-4}$  (for this see also section 6). Therefore, the direct measurement of the power-law dependence of the visibility for large bias voltages seems to be a challenging task, unless one finds a way to optimize further the relevant parameters.

## 5. Keldysh perturbation theory

### 5.1. General remarks

The semiclassical method we introduced in the preceding section provides us with an intuitive picture for the case of electrons flying high above the Fermi sea. To complete the analysis, in the present section we employ perturbation theory to discuss the behavior at short propagation distances and weak coupling for all energies. This includes the low energy regime, where the influence of the Fermi edge becomes important. We will apply Keldysh (i.e. nonequilibrium) perturbation theory up to second order in the interaction strength  $\alpha$ . The main outcome of the perturbation theory is that the tunnel density of states is affected by renormalization effects while the decay of the GF in the close vicinity of the Fermi edge is suppressed. We will find that the suppression of decoherence is brought about by a cancellation between two second-order diagrams near the Fermi edge.

During this subsection we fix the notation, following the review [41]. Using the Keldysh time leads to an additional matrix structure of the GF which reflects the fact that one has to differentiate between points in time which lie on the backward or the forward branch of the Keldysh contour. Beyond this additional structure, all the known Feynman rules remain exactly the same. After performing the rotation in Keldysh space [41], the representation of the matrix GF  $G$  and the related matrix self-energy is given by

$$G \equiv \begin{bmatrix} G^R & G^K \\ 0 & G^A \end{bmatrix}, \quad \Sigma \equiv \begin{bmatrix} \Sigma^R & \Sigma^K \\ 0 & \Sigma^A \end{bmatrix}, \quad (63)$$

where we introduce the Keldysh GF,  $G^K(x, t, x', t') \equiv -i\langle[\hat{\Psi}(x, t), \hat{\Psi}^\dagger(x', t')]\rangle$ . First, we will derive an expression for the retarded self-energy  $\Sigma^R(\epsilon, k)$ , which will be used to calculate  $G^R$  that can be related to the single particle propagator  $G^>$  in equilibrium. Starting from the matrix Dyson equation  $G(\epsilon, k) = G_0(\epsilon, k) + G_0(\epsilon, k) \cdot \Sigma(\epsilon, k) \cdot G(\epsilon, k)$ , one finds that the retarded GF only depends on the retarded self-energy:

$$G^R(\epsilon, k) = \frac{1}{[\epsilon - \epsilon_0(k) + i0^+] - \Sigma^R(\epsilon, k)}. \quad (64)$$

In the following, we calculate the diagrams up to second order for a linearized dispersion relation, but for finite temperature and for an arbitrary interaction potential. In the end, we compare the results of the perturbation theory with the results of the bosonization technique. The relevant processes are shown in figure 7. There are two second-order diagrams, which can be identified as the interaction with a plasmonic excitation and a corresponding diagram containing an additional exchange process (that can be viewed as a vertex correction diagram). The crucial point is that the vertex correction counteracts the plasmonic processes in the vicinity of the Fermi edge, leading to a suppression of the decay of the GF.

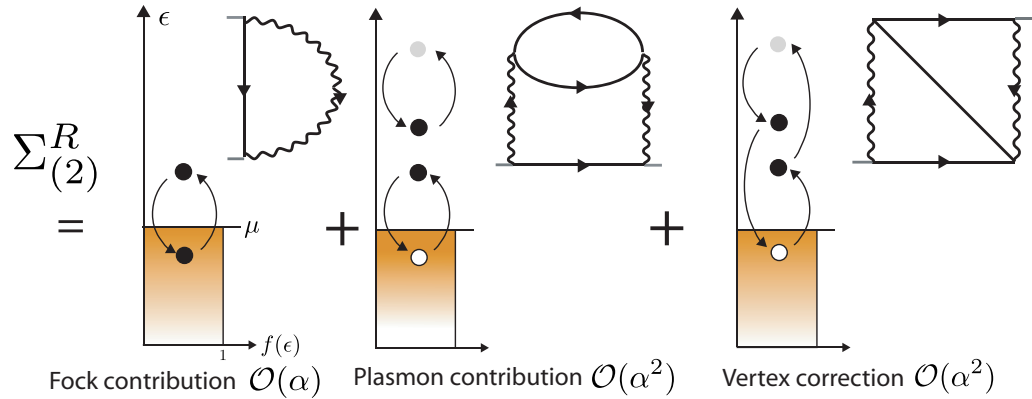


**Figure 7.** The relevant processes which contribute to the self-energy up to second order in the coupling. The wiggly lines indicate the interaction. Note that the plasmonic diagram and the vertex correction differ only by an additional exchange process. That produces a minus sign, such that the diagrams tend to cancel each other at low momenta.

## 5.2. Evaluation of the diagrams

The starting point of the calculation is the evaluation of the unperturbed electronic propagator matrix  $G_0$ . In addition to the usual retarded and advanced GFs of free electrons,  $G_0^{R/A}(\omega, k) = \frac{1}{\omega - v_F k \pm i0^+}$ , the Keldysh propagator is given by  $G_0^K(\omega, k) = -2\pi i \tanh(\frac{\beta\omega}{2}) \cdot \delta(\omega - v_F k)$ . In contrast to the advanced and retarded GFs, the Keldysh propagator contains information about the electronic spectrum as well as about the occupation of those states. Therefore at this point one could introduce arbitrary non-equilibrium states which is the main advantage of working on the Keldysh contour. However, as we are describing channels which are only weakly tunnel-coupled to each other, we will calculate equilibrium GFs.

As in second order we explicitly include interactions with free plasmons, we also derive their propagators here. To this end we identify the bosonic field with the potential  $\hat{V}(x, t) = \int dx' U(x - x') \hat{\rho}(x', t)$ . This is identical to the potential we introduced in the semiclassical description (although in the latter case we specialized to  $x \equiv v_F t$ ). The bosonic propagators are defined as  $D^{R/A}(x, t) = \mp i\theta(\pm t) \langle [\hat{V}(x, t), \hat{V}(0, 0)] \rangle$  and  $D^K(x, t) = -i \langle \{\hat{V}(x, t), \hat{V}(0, 0)\} \rangle$ , respectively. A straightforward calculation yields for the retarded and advanced propagators

$$D^{R/A}(\omega, q) = U_q^2 \int \frac{dk}{2\pi} \frac{f(k) - f(q+k)}{(\omega + \epsilon_0(k) - \epsilon_0(k+q)) \pm i0^+} = U_q^2 \frac{q}{2\pi} G^{R/A}(\omega, q). \quad (65)$$

As we assume the system to be in equilibrium, we use the FDT to obtain the plasmonic Keldysh propagator:

$$D^K(\omega, q) = 2i \coth(\beta\omega/2) \text{Im}[D^R(\omega, q)]. \quad (66)$$

Now we can proceed calculating the various contributions to the self-energy up to  $\mathcal{O}(\alpha^2)$ . Considering all the possible Feynman diagrams, we are left with the first-order Hartree–Fock diagrams and in second order with the plasmon diagram and the vertex correction (see figure 7). Thus we can express the self-energy as  $\Sigma_{(2)}^R = \Sigma_{\text{Hartree}} + \Sigma_{\text{Fock}} + \Sigma_{\text{Plasmon}} + \Sigma_{\text{Vertex}}$ . Those can be

evaluated according to the rules given in [41]. We use the equal-time interaction propagators  $U^{\text{R/A}}(q) \equiv U_q$  and set  $U^{\text{K}} \equiv 0$ , as usual.

*5.2.1. First-order contributions: Hartree–Fock diagrams.* The Hartree diagram yields a global energy renormalization  $\Delta E_{\text{Hartree}} = U(q=0)\bar{\rho}$ . In the framework of the Luttinger model the electron density diverges as there is no lower boundary of the electron spectrum. However, formally one can include the energy shift into the definition of the chemical potential (see section 3.1). In the following we omit the Hartree contribution.

The self-energy contribution due to the Fock diagrams is

$$\Sigma_{\text{F}}^{\text{R}}(\omega, k) = -\frac{1}{2\pi} \int dq U_q f(k-q), \quad (67)$$

which for zero temperature yields  $\Sigma_{\text{F}, T=0}^{\text{R}}(k) = -\frac{1}{2}U(x=0) + \frac{1}{2\pi} \int_0^{|k|} dq U_q$  (see figure 8(b)).

The resulting  $k$ -dependent energy shift describes, in particular, the renormalization of the electron velocity near the Fermi edge. This also affects the tunneling density of states, leading to a suppression (for repulsive interactions,  $\alpha > 0$ ) or enhancement ( $\alpha < 0$ ). This can be seen in figure 3. Again, the constant shift can be incorporated in the definition of the chemical potential.

*5.2.2. Second-order contributions: plasmonic excitations and vertex correction.* The electron's coherence decays by interacting with the plasmons, i.e. the density fluctuations of the other electrons. The plasmon diagram (see figure 7) represents one of the contributions describing this physics. It yields

$$\Sigma_{\text{P}}^{\text{R}}(\epsilon, k) = \frac{i}{2} \int (dq) \int (d\omega) [G_0^{\text{R}}(\epsilon - \omega, k - q) \cdot D_0^{\text{K}}(\omega, q) + G_0^{\text{K}}(\epsilon - \omega, k - q) \cdot D_0^{\text{R}}(\omega, q)], \quad (68)$$

where the second term contains the Fermi function, which introduces the effects of the Fermi edge on the coherence. Inserting the propagators, the contribution can be written in a compact form

$$\Sigma_{\text{P}}^{\text{R}}(\epsilon, k) = \frac{G_0^{\text{R}}(\epsilon, k)}{8\pi^2} \int_{-\infty}^{\infty} dq U_q^2 q \cdot [\coth(\beta\hbar v_{\text{F}}q/2) + \tanh(\beta\hbar v_{\text{F}}(k-q)/2)], \quad (69)$$

which for  $T = 0$  reduces to  $\Sigma_{\text{P}}^{\text{R}}(\epsilon, k) = G_0^{\text{R}}(\epsilon, k) \cdot \frac{1}{4\pi^2} \int_0^{|k|} dq U_q^2 q$ . Thus, at  $T = 0$  this contribution vanishes for  $k \rightarrow 0$ . We note in passing that the structure ‘coth + tanh’ generically occurs in discussions of dephasing, where it describes both the strength of the thermal fluctuations and the influence of the Fermi function, i.e. the physics of Pauli blocking [8]–[10], [17, 21, 42]. In the limit of high energies, the result of equation (69) can be rewritten in terms of the potential fluctuations at the particle position, as discussed in the preceding section. Specifically, we have  $\lim_{k \rightarrow \infty} \Sigma_{\text{P}, T=0}^{\text{R}} = G_0^{\text{R}} \cdot \langle \hat{V}(x=0, t=0)^2 \rangle$ . For a plot of the function  $\Sigma_{\text{P}, T=0}^{\text{R}}$ , see figure 8(c).

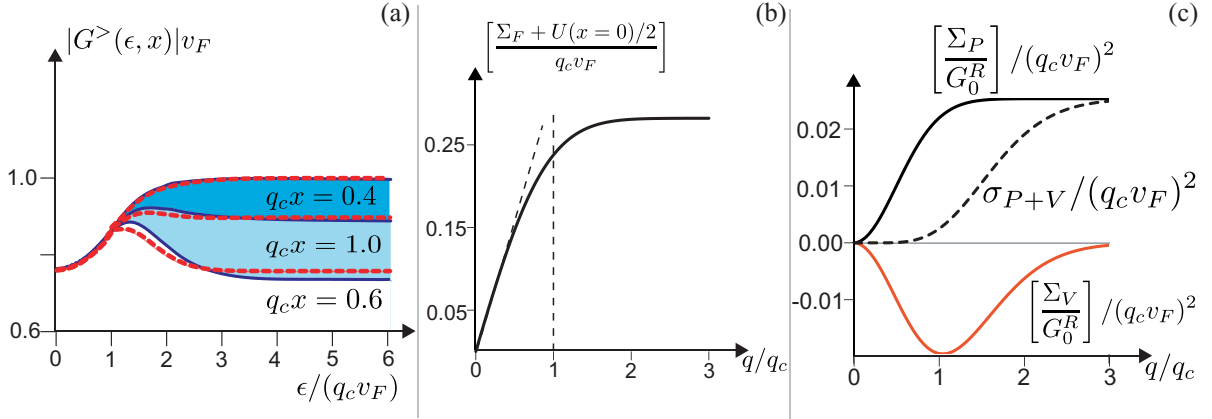


**Figure 8.** (a) The GF from bosonization (solid blue lines) versus the results from second-order Keldysh perturbation theory (dashed red lines) for different propagation distances as a function of energy. Note the fairly good agreement. (b) Fock contribution to the self-energy  $\Sigma_F^R(k)$ , which starts with a linear slope (corresponding to the electron velocity renormalization) and then saturates for large momenta. (c) Total second-order contribution the self-energy (dashed, black line); plasmonic (solid black line) and vertex correction (lower, red line) separately. The cancellation for small momenta is discussed in detail in the text (in all figures  $U_q = U_0 \exp(-(q/q_c)^2)$  and  $2\pi\alpha = U_0/v_F = 2$ ).

Finally we derive the vertex correction, mentioned above, which after a rather lengthy calculation yields (see appendix B)

$$\begin{aligned} \Sigma_V^R(\epsilon, k) = & \left[ \frac{G_0^R(\epsilon, k)}{16\pi^2} \right] \int_{-\infty}^{\infty} dq_1 \int_{-\infty}^{\infty} dq_2 U_{q_1} U_{q_2} \\ & \times \left[ \tanh\left(\frac{\beta v_F(k - q_1 - q_2)}{2}\right) \left[ \tanh\left(\frac{\beta v_F(k - q_1)}{2}\right) + \tanh\left(\frac{\beta v_F(k - q_2)}{2}\right) \right] \right. \\ & \left. - \tanh\left(\frac{\beta v_F(k - q_2)}{2}\right) \tanh\left(\frac{\beta v_F(k - q_1)}{2}\right) - 1 \right]. \end{aligned} \quad (70)$$

This expression simplifies for  $T = 0$  to  $\Sigma_{V, T=0}^R = -G_0^R \cdot \frac{1}{4\pi^2} \int_0^{|k|} dq_1 \int_{|k|-q_1}^{|k|} dq_2 U_{q_1} U_{q_2}$ . The contribution from the vertex correction as well as the total second-order correction to the self-energy  $\sigma_{P+V}^R \equiv \Sigma_P^R + \Sigma_V^R$  are shown in figure 8. The crucial feature is that up to second order in momentum  $k$  the plasmon diagram and the vertex correction cancel exactly against each other, whereas for high momenta [ $k \gg q_c$ ] only the plasmon contribution remains while the vertex correction tends to zero. In summary, when calculating up to second order in the coupling, we already see that the dephasing is suppressed in the vicinity of the Fermi edge. As the comparison with the exact bosonization solution shows, this conclusion holds true qualitatively to all orders. We can use the preceding expressions to evaluate the retarded GF  $G^R$  and from this the propagator  $G^>$ . The final results has evaluated numerically. The results are illustrated in figure 8. Expanding the GF for small propagation distance  $x \ll v_F(2\sqrt{\langle \hat{V}(0)^2 \rangle})^{-1}$ , yields:

$$|G^>(\epsilon \rightarrow \infty, x)|v_F \approx 1 - \frac{1}{2} \langle \hat{V}(0)^2 \rangle \left( \frac{x}{v_F} \right)^2 + \dots, \quad (71)$$

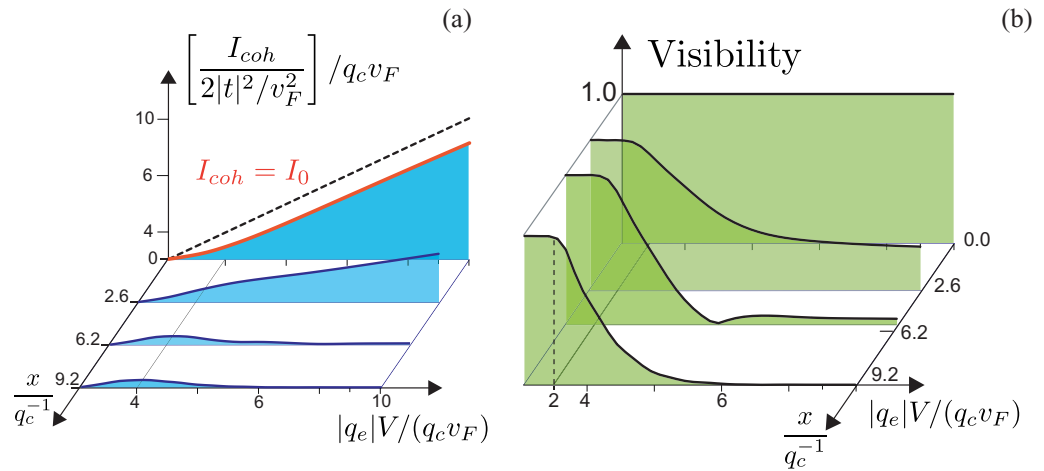


**Figure 9.** (a) The amplitude of the coherent (flux-dependent) part of the current  $I_{coh}$  through the interferometer for different arm lengths  $x$ . The curve for  $x \equiv 0$  is equal to the flux-independent current  $I_{coh}(x \equiv 0, V) = I_0(V)$  (red line), which implies that the interference contrast is perfect at zero arm length. (b) The visibility  $v_I$  as a function of bias voltage  $V$  for various arm-lengths  $x_1 = x_2 = x$ . The red line denotes the semiclassical calculation. The small deviations from the bosonization result vanish completely for larger  $V$ . The plot is done for  $U_q = U_0 e^{-(q/q_c)^2}$  with  $\frac{U_0}{v_F} = 2\pi\alpha = 3$ .

which coincides with the expanded exact result. The good agreement of the bosonization result and the Keldysh perturbation theory for small  $|\alpha|$  is shown in figure 8, as well as in figure 5. However, for large  $x$  the perturbation theory fails.

For a detailed study of chiral interacting electrons of the spectrum in  $(\epsilon - k)$ -space, starting from the bosonization result, we refer the reader to [34].

### 5.3. Summary of the Keldysh perturbation theory

To summarize, the perturbation theory shows that there are two different energy regimes: in general, the GF decays as a function of propagation distance due to the interaction with the density fluctuations. This is particularly pronounced at high energies  $\epsilon \gg v_F q_c$ , where we have also shown that the Keldysh result and the semiclassical (or bosonization) approach coincide at short distances. For low energies  $\epsilon \ll v_F q_c$ , the decay is suppressed. On the other hand, at low energies the Fermi velocity is renormalized due to virtual processes, leading to a modification of the tunneling density of states. It is important to note that these two different energy regimes only emerge since we are dealing with interaction potentials of finite range.

## 6. Visibility and current

As mentioned in the beginning, the results for the GF  $G^>(\epsilon, x)$  we worked out in the foregoing section can be applied directly to the evaluation of the current and the visibility (figure 9).

Figure 9(a) shows the current through the interferometer as a function of voltage for different arm lengths. Here we restrict the considerations to the symmetric case, i.e.  $x_1 = x_2$ .

For  $x = 0$  the coherent part of the current obviously is identical to the flux-independent part, which implies a perfect visibility (at  $T = V = 0$ ). The suppression of the current at small voltages is due to the velocity renormalization which lowers the tunnel density (for repulsive interactions). However, as the change in the tunnel density influences the classical and the coherent part in the same way, it does not show up in the visibility at all, i.e.  $v_I(V, x = 0) \equiv 1$  (see figure 9(b)).

The behavior of the coherence of the GF for high energies discussed above (using the semiclassical approach) can be transferred directly to the discussion of the visibility. Therefore, in the limit of high voltages  $V$  and  $T = 0$  the visibility is determined by the factor  $|G^>(\epsilon \rightarrow \infty, x)|^2$ . This follows from the fact that for higher voltages the contribution of the high-energy electrons becomes dominant. It also implies that the visibility at high voltages becomes voltage-independent. Correspondingly, the exponential decay at finite temperature is transferred to the visibility  $v_I$  as well. For  $x \neq 0$  the dephasing reduces the coherent (flux-dependent) part of the current which leads to a decrease of the visibility. At small voltages  $|q_e V| \ll q_c v_F$  the visibility decays only very slowly with increasing interferometer length (see the discussion of the GF). In the limit  $V \rightarrow 0$  the visibility is approaching unity  $v_I \rightarrow 1$ , which is consistent with the fact that in equilibrium and at zero temperature there is no dephasing. In contrast to the GF itself, which shows oscillations as a function of  $\epsilon$ , the visibility does not show pronounced oscillations as a function of  $V$ .

## 7. Conclusions

In the present paper, we have studied dephasing by electron–electron interactions in a ballistic interferometer. We have considered the case of electrons moving inside ballistic, 1D, chiral channels, such as edge channels in the integer QHE. The interference contrast, in the limit of low transmission at the beam splitters, can be expressed via the GF of the interacting system. We have studied the decay of the electron’s coherence as a function of propagation distance, employing three different approaches: the exact bosonization solution, a semiclassical approach that becomes exact for high energies, and diagrammatic nonequilibrium (Keldysh) perturbation theory. Our most important physical result is that at high energies the decay of coherence at  $T = 0$  becomes a power-law with a universal exponent, independent of interaction strength. We have also shown that second-order perturbation theory compares well with the exact solution at modest coupling strength and short distances. This may be important for potential applications to more elaborate setups that cannot be treated exactly any more.

## Acknowledgments

We thank J Chalker, Y Gefen, V Meden, B Kubala and O Yevtushenko for interesting discussions related to this work. Financial support by DIP, NIM, the Emmy-Noether program and the SFB/TR 12 is gratefully acknowledged.

## Appendix A. Semiclassical approach

### A.1. Amplitude of the oscillations in $G^>(\epsilon, x)$ as a function of $x$ for $T = 0$

The third term in equation (57) is responsible for the oscillations in  $G^>(\epsilon \rightarrow \infty, x)$ , while the main contribution stems from the square-root singularity at  $\omega = |\omega_{\max}|$ . This contribution

yields:

$$\begin{aligned} \delta F(x) &= 2 \int_{|\omega_{\max}|-\delta}^{|\omega_{\max}|} (d\omega) \frac{\sin^2(\omega x/(2v_F))}{\omega^2} \langle \{ \hat{V}, \hat{V} \} \rangle_{\omega \approx |\omega_{\max}|} \\ &= \text{const.} - \text{Re} \left[ \int_{|\omega_{\max}|-\delta}^{|\omega_{\max}|} (d\omega) \frac{e^{i\omega(x/v_F)}}{\omega^2} \langle \{ \hat{V}, \hat{V} \} \rangle_{\omega \approx |\omega_{\max}|} \right]. \end{aligned} \quad (\text{A.1})$$

From equation (53) we obtain the  $\omega$ -dependence of the correlator in the vicinity of the singularity

$$\langle \{ \hat{V}, \hat{V} \} \rangle_{\omega} \approx \frac{1}{2\pi} \frac{U^2(q_0)q_0}{2\sqrt{|\xi|(|\omega_{\max}|-\omega)}}, \quad (\text{A.2})$$

where  $\omega(q^*) = \max(|\omega_q - v_F q|)$ ,  $q_0 \equiv q^* + \sqrt{\frac{|\omega_{\max}|-\omega}{|\xi|}}$  and  $\xi \equiv \frac{1}{2} \frac{d^2}{dq^2} \left( \frac{|U_q|q}{2\pi} \right)_{q=q^*}$ . Plugging in this result into equation (A.1) yields

$$\begin{aligned} \delta F &\approx -\frac{1}{8\pi^2} \frac{U^2(q^*)q^*}{\omega_{\max}^2 \sqrt{|\xi|}} \text{Re} \left[ \int_{|\omega_{\max}|-\delta}^{|\omega_{\max}|} d\omega \frac{e^{i\omega(x/v_F)}}{\sqrt{|\omega_{\max}|-\omega}} \right] \\ &= -\frac{1}{8\pi^2} \frac{U^2(q^*)q^*}{\omega_{\max}^2 \sqrt{|\xi|}} \text{Re} \left[ \int_0^{\delta(x/v_F)} dv \frac{e^{iv}}{\sqrt{v}} \frac{e^{i|\omega_{\max}|(x/v_F)}}{\sqrt{t}} \right]. \end{aligned} \quad (\text{A.3})$$

Evaluating the integral in the limit  $x \rightarrow \infty$  gives

$$\begin{aligned} \delta F(x) &\approx -\left[ \frac{1}{8\pi^2} \frac{U^2(q^*)q^*}{\omega_{\max}^2 \sqrt{|\xi|}} \right] \sqrt{\frac{\pi}{t}} \sin \left( |\omega_{\max}| \frac{x}{v_F} + \pi/4 \right) \\ &= -C \frac{\sin(|\omega_{\max}|(x/v_F) + \pi/4)}{\sqrt{2\pi} |\alpha| q_c x}, \end{aligned} \quad (\text{A.4})$$

where  $C$  denotes a numerical prefactor which depends only on the form of the interaction potential, not on the interaction strength  $\alpha$ .

#### A.2. Sub-leading corrections for smooth potentials $U_q$ at $T = 0$

The subleading corrections result from the contributions of large  $q$  in equation (53) (here  $\omega > 0$ ). We start with the expression

$$\langle \{ \hat{V}, \hat{V} \} \rangle_{\omega} = \int_0^{\infty} dq U_q^2 q \delta \left( \omega - \frac{q|U_q|}{2\pi} \right). \quad (\text{A.5})$$

The sub-leading correction to the low-frequency behavior of  $\langle \{ \hat{V}, \hat{V} \} \rangle_{\omega}$  for a smooth potential  $U_q = U_0 e^{-|q/q_c|^s}$  is given by

$$\langle \{ \hat{V}, \hat{V} \} \rangle_{\omega}^{(\text{sub})} = \int_0^{\infty} dq U_q^2 q \frac{\delta(q - q_{\text{sub}})}{\left| \frac{\partial}{\partial q} (|U_q|q) \right|_{q=q_{\text{sub}}}}, \quad (\text{A.6})$$

where  $q_{\text{sub}}$  fulfills:  $\frac{2\pi\omega}{|U_0|q_c} = \frac{q_{\text{sub}}}{q_c} e^{-|q_{\text{sub}}/q_c|^s}$ . Therefore, as  $q \gg q_c$  for  $\omega$  small enough we obtain for  $q_{\text{sub}}$

$$q_{\text{sub}} = q_c \ln \left[ \frac{q_c |U_0|}{2\pi\omega} \right]^{1/s}. \quad (\text{A.7})$$

Finally, the subleading corrections yield

$$\left\langle \left\{ \hat{V}, \hat{V} \right\} \right\rangle_{\omega}^{(\text{sub})} = \frac{2\pi\omega}{s \ln\left(\frac{|\alpha|v_F q_c}{\omega}\right)}, \quad (\text{A.8})$$

for  $\omega \ll |\alpha|v_F q_c$ .

### A.3. Sub-leading correction in time-domain for $T = 0$

The subleading correction to the decay function  $F(x)$  results from the expression  $F^{(\text{sub})} = \int_{-\infty}^{\infty} \frac{d\omega}{2\pi} \frac{\sin^2(\omega x/(2v_F))}{\omega^2} \cdot \left\langle \left\{ \hat{V}, \hat{V} \right\} \right\rangle_{\omega}^{(\text{sub})}$ . With equation (A.8) (omitting an additional constant) it yields

$$F^{(\text{sub})}(x) \approx \frac{2}{2} \int_{v_F/x}^{\omega_c} (d\omega) \frac{2\pi\omega}{\omega s \ln(\omega^*/\omega)} = -\frac{1}{s} \int_{v_F/(\omega^*x)}^{\omega_c/\omega^*} d\omega \frac{1}{\omega \ln \omega}, \quad (\text{A.9})$$

where for reasons of brevity we set  $|\alpha|v_F q_c \equiv \omega^*$ . As we can choose the cutoff frequency  $\omega_c$  such that  $\omega_c/\omega^* < 1$ , we can assume  $0 < \omega < 1$ . This enables the substitution  $\omega = e^{-x}$ :

$$\begin{aligned} F^{(\text{sub})}(t) &= -\frac{1}{s} \int_{\ln(\omega^*x/v_F)}^{\ln(\omega^*/\omega_c)} dx \frac{1}{x} \\ &= \frac{1}{s} \int_{\ln(\omega^*/\omega_c)}^{\ln(\omega^*x/v_F)} dx \frac{1}{x} = \frac{1}{s} \ln(\ln(|\alpha|q_c x)) - \text{const.} \end{aligned} \quad (\text{A.10})$$

## Appendix B. Keldysh perturbation theory: vertex correction

The vertex correction to the retarded self-energy has the structure (compare to the review of [41]):

$$\begin{aligned} \Sigma_V(\epsilon, k) &= \left(\frac{i}{2}\right)^2 \frac{1}{(2\pi)^4} \int dk_1 \int dk_2 \int d\omega_1 \int d\omega_2 U_{q_1} U_{q_2} \\ &\quad \times [ G_0^R(\epsilon - \omega_2, k - k_2) G_0^K(\epsilon - \omega_1 - \omega_2, k - k_1 - k_2) G_0^K(\epsilon - \omega_1, k - k_1) \\ &\quad + G_0^R(\epsilon - \omega_2, k - k_2) G_0^A(\epsilon - \omega_1 - \omega_2, k - k_1 - k_2) G_0^R(\epsilon - \omega_1, k - k_1) \\ &\quad + G_0^K(\epsilon - \omega_2, k - k_2) G_0^K(\epsilon - \omega_1 - \omega_2, k - k_1 - k_2) G_0^R(\epsilon - \omega_1, k - k_1) \\ &\quad + G_0^K(\epsilon - \omega_2, k - k_2) G_0^A(\epsilon - \omega_1 - \omega_2, k - k_1 - k_2) G_0^K(\epsilon - \omega_1, k - k_1) ]. \end{aligned} \quad (\text{B.1})$$

## References

- [1] Weiss U 2000 *Quantum Dissipative Systems* (Singapore: World Scientific)
- [2] Zurek W 1991 Decoherence and the transition from quantum to classical *Phys. Today* **44** 36
- [3] Joos E *et al* 2003 *Decoherence and the Appearance of a Classical World in Quantum Theory* (Heidelberg: Springer)
- [4] Braginsky V B and Khalili F Y 1992 *Quantum Measurement* (Cambridge: Cambridge University Press)
- [5] Leggett A J, Chakravarty S, Dorsey A T, Fisher M P A, Garg A and Zwerger W 1987 Dynamics of the dissipative two-state system *Rev. Mod. Phys.* **59** 1

- [6] Neder I and Marquardt F 2007 Coherence oscillations in dephasing by non-gaussian shot noise *New J. Phys.* **9** 112
- [7] Abel B and Marquardt F 2008 Decoherence by quantum telegraph noise arXiv:0805.0962
- [8] Marquardt F, Delft J v, Smith R and Ambegaokar V 2007 Decoherence in weak localization I: Pauli principle in influence functional *Phys. Rev. B* **76** 195331
- [9] Delft J v, Marquardt F, Smith R and Ambegaokar V 2007 Decoherence in weak localization II: Bethe–Salpeter calculation of Cooperon *Phys. Rev. B* **76** 195332
- [10] Marquardt F 2007 Decoherence of fermions subject to a quantum bath *Advances in Solid State Physics* vol 46 ed R Haug (Berlin: Springer) (arXiv:cond-mat/0604626)
- [11] Ji Y, Chung Y, Sprinzak D, Heiblum M, Mahalu D and Shtrikman H 2003 An electronic Mach–Zehnder interferometer *Nature* **422** 415
- [12] Neder I, Heiblum M, Levinson Y, Mahalu D and Umansky V 2006 Unexpected behavior in a two-path electron interferometer *Phys. Rev. Lett.* **96** 016804
- [13] Neder I, Marquardt F, Heiblum M, Mahalu D and Umansky V 2007 Controlled dephasing of electrons by non-gaussian shot noise *Nat. Phys.* **3** 534
- [14] Litvin L V, Helzel A, Tranitz H P, Wegscheider W and Strunk C 2008 Edge-channel interference controlled by Landau level filling *Phys. Rev. B* **78** 075303
- [15] Roulleau P, Portier F, Roche P, Cavanna A, Faini G, Gennser U and Mailly D 2008 Direct measurement of the coherence length of edge states in the integer quantum hall regime *Phys. Rev. Lett.* **100** 126802
- [16] Marquardt F and Bruder C 2004 Influence of dephasing on shot noise in an electronic Mach–Zehnder interferometer *Phys. Rev. Lett.* **92** 056805
- [17] Marquardt F 2005 Fermionic Mach–Zehnder interferometer subject to a quantum bath *Europhys. Lett.* **72** 788
- [18] Marquardt F and Bruder C 2004 Effects of dephasing on shot noise in an electronic Mach–Zehnder interferometer *Phys. Rev. B* **70** 125305
- [19] Förster H, Pilgram S and Büttiker M 2005 Decoherence and full counting statistics in a Mach–Zehnder interferometer *Phys. Rev. B* **72** 075301
- [20] Chung V S-W, Samuelsson P and Buttiker M 2005 Visibility of current and shot noise in electrical Mach–Zehnder and Hanbury Brown–Twiss interferometers *Phys. Rev. B* **72** 125320
- [21] Marquardt F 2006 Equations of motion approach to decoherence and current noise in ballistic interferometers coupled to a quantum bath *Phys. Rev. B* **74** 125319
- [22] Seelig G and Büttiker M 2001 Charge-fluctuation-induced dephasing in a gated mesoscopic interferometer *Phys. Rev. B* **64** 245313
- [23] Law K T, Feldman D E and Gefen Y 2006 Electronic Mach–Zehnder interferometer as a tool to probe fractional statistics *Phys. Rev. B* **74** 045319
- [24] Sukhorukov E V and Cheianov V V 2007 Resonant dephasing of the electronic Mach–Zehnder interferometer *Phys. Rev. Lett.* **99** 156801
- [25] Chalker J T, Gefen Y and Veillette M Y 2007 Decoherence and interactions in an electronic Mach–Zehnder interferometer *Phys. Rev. B* **76** 085320
- [26] Neder I and Ginossar E 2008 Behavior of electronic interferometers in the nonlinear regime *Phys. Rev. Lett.* **100** 196806
- [27] Levkivskiy I P and Sukhorukov E V 2008 Dephasing in the electronic Mach–Zehnder interferometer at filling factor  $\nu = 2$  *Phys. Rev. B* **78** 045322
- [28] Apel W and Rice T M 1983 Localisation and interaction in one dimension *J. Phys. C: Solid State Phys.* **16** L271
- [29] Le Hur K 2002 Electron fractionalization-induced dephasing in Luttinger liquids *Phys. Rev. B* **65** 233314

- [30] Le Hur K 2005 Dephasing of mesoscopic interferences from electron fractionalization *Phys. Rev. Lett.* **95** 076801
- [31] Gornyi I V, Mirlin A D and Polyakov D G 2005 Dephasing and weak localization in disordered Luttinger liquid *Phys. Rev. Lett.* **95** 046404
- [32] Le Hur K 2006 Electron lifetime in Luttinger liquids *Phys. Rev. B* **74** 165104
- [33] Gutman D B, Gefen Y and Mirlin A 2008 Non-equilibrium Luttinger liquid: zero-bias anomaly and dephasing *Phys. Rev. Lett.* **101** 126802
- [34] Meden V and Schoenhammer K 1993 Nonuniversal spectral properties of the Luttinger model *Phys. Rev. B* **47** 16205–15
- [35] Meden V 1999 Nonuniversality of the one-particle Green's function of a Luttinger liquid *Phys. Rev. B* **60** 4571–5
- [36] Neuenhahn C and Marquardt F 2008 Universal dephasing in a chiral 1D interacting fermion system arXiv:0806.121
- [37] Delft J v and Schoeller H 1998 Bosonization for beginners—refermionization for experts *Ann. Phys.* **4** 225
- [38] Giamarchi T 2006 *Quantum Physics in One Dimension* (Oxford: Oxford University Press)
- [39] Mahan G D 2000 *Many-Particle Physics* (New York: Kluwer)
- [40] Marquardt F and Bruder C 2002 Aharonov–Bohm ring with fluctuating flux *Phys. Rev. B* **65** 125315
- [41] Smith H and Rammer J 1986 Quantum field-theoretical methods in transport theory of metals *Rev. Mod. Phys.* **58** 323–59
- [42] Fukuyama H and Abrahams E 1983 Inelastic scattering time in two-dimensional disordered metals *Phys. Rev. B* **27** 5976